AD-A126 672 THEORETICAL PROPERTIES OF ACOUSTICAL SPECKLE INTERFEROMETRY(U) ARMY MISSILE COMMAND REDSTONE ARSENAL AL GROUND EQUIPMENT AND.. W F RANSON SEP 80 1/1

UNCLASSIFIED DRSMI/RL-81-5-TR SBI-AD-E950 372 F/G 20/1 NL

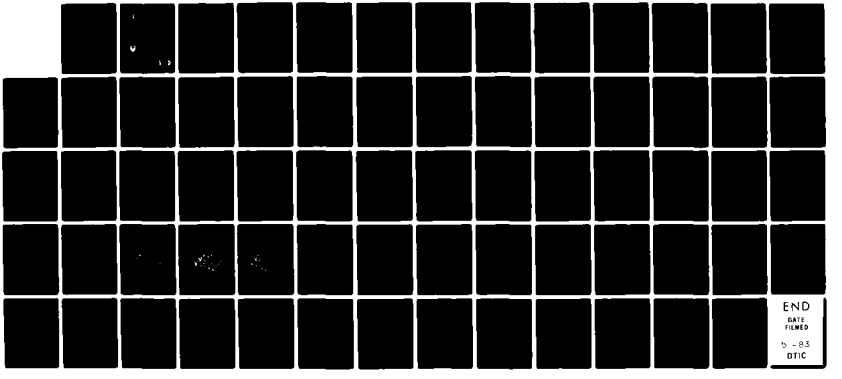

END
DATE FILMED
5-83
DTIC

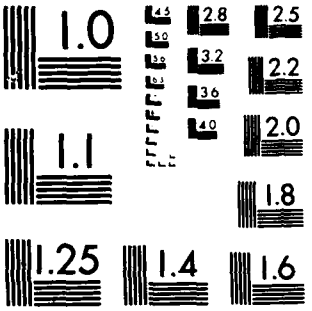

TECHNICAL REPORT RL-81-5

THEORETICAL PROPERTIES OF ACOUSTICAL SPECKLE INTERFEROMETRY

W. F. Ranson
College of Engineering
University of South Carolina
Columbia, South Carolina 29208

For

Ground Equipment and Missile Structures Directorate
US Army Missile Laboratory

September 1980

U.S. ARMY MISSILE COMMAND
Redstone Arsenal, Alabama 35898

Approved for public release; distribution unlimited.

DISPOSITION INSTRUCTIONS

DESTROY THIS REPORT WHEN IT IS NO LONGER NEEDED. DO NOT RETURN IT TO THE ORIGINATOR.

DISCLAIMER

THE FINDINGS IN THIS REPORT ARE NOT TO BE CONSTRUED AS AN *OFFICIAL DEPARTMENT OF THE ARMY POSITION* UNLESS SO DESIGNATED BY OTHER AUTHORIZED DOCUMENTS.

TRADE NAMES

USE OF TRADE NAMES OR MANUFACTURERS IN THIS REPORT DOES NOT CONSTITUTE AN OFFICIAL INDORSEMENT OR APPROVAL OF THE USE OF SUCH COMMERCIAL HARDWARE OR SOFTWARE.

UNCLASSIFIED

SECURITY CLASSIFICATION OF THIS PAGE (When Data Entered)

REPORT DOCUMENTATION PAGE	READ INSTRUCTIONS BEFORE COMPLETING FORM
1. REPORT NUMBER: TR-RL-81-5	2. GOVT ACCESSION NO.: AD-A126 672
3. RECIPIENT'S CATALOG NUMBER:	
4. TITLE (and Subtitle): Theoretical Properties of Acoustical Speckle Interferometry	5. TYPE OF REPORT & PERIOD COVERED: Technical Report
	6. PERFORMING ORG. REPORT NUMBER:
7. AUTHOR(s): W. F. Ranson	8. CONTRACT OR GRANT NUMBER(s): DA1L162303A214
9. PERFORMING ORGANIZATION NAME AND ADDRESS: Commander, US Army Missile Command, ATTN: DRSMI-RL, Redstone Arsenal, Alabama 35898	10. PROGRAM ELEMENT, PROJECT, TASK AREA & WORK UNIT NUMBERS: AMCMS 6123032140911
11. CONTROLLING OFFICE NAME AND ADDRESS: Commander, US Army Missile Command, ATTN: DRSMI-RPT, Redstone Arsenal, Alabama 35898	12. REPORT DATE: 30 September 1980
	13. NUMBER OF PAGES:
14. MONITORING AGENCY NAME & ADDRESS(if different from Controlling Office)	15. SECURITY CLASS. (of this report): Unclassified
	15a. DECLASSIFICATION/DOWNGRADING SCHEDULE:

16. DISTRIBUTION STATEMENT (of this Report)

Approved for public release; distribution unlimited.

17. DISTRIBUTION STATEMENT (of the abstract entered in Block 20, if different from Report)

18. SUPPLEMENTARY NOTES

This work was accomplished through the LRCP Program between Dr. W. F. Ranson and the US Army Missile Command.

19. KEY WORDS (Continue on reverse side if necessary and identify by block number)

Acoustical Speckle Interferometry
Laser Speckle Interferometry
Interferometry
Acoustics
Non-destructive Testing

20. ABSTRACT (Continue on reverse side if necessary and identify by block number)

Acoustical speckle interferometry is based locally on the elastodynamic response of solids subjected to ultrasonic waves. The presence of a subsurface layer or disconunity generally produces a change in the wave propagating in a medium. Acoustical speckle interferometry utilizes the reflection, refraction, and mode conversion of incident elastic waves at the interface of two elastic media as a basic description of the transmission and reflection of elastic waves.

Basic equations for the reflection and refraction of a layered elastic half space are derived. Numerical examples of liquid-solid and solid interfaces are

DD FORM 1 JAN 73 1473 EDITION OF 1 NOV 65 IS OBSOLETE

UNCLASSIFIED

SECURITY CLASSIFICATION OF THIS PAGE (When Data Entered)

Item #20 (Cont)

presented. A two-layer solid medium immersed in water is solved to illustrate the effect of an incident p-wave on the refraction and reflection properties.

Theoretical properties of acoustical speckle interferometry are discussed which includes the effect of deformation. A data analysis procedure is described which utilizes a two-dimensional correlation of acoustical signals as a direct measure of object motion. Numerical examples are presented to illustrate the correlation of reference and deformed ultrasonic signals. Uniform translations without geometric distortion are presented. Geometric distortions for both infinitesimal and finite deformations are illustrated to show this effect on the deformed acoustical surface. All results are presented in graphical form.

TABLE OF CONTENTS

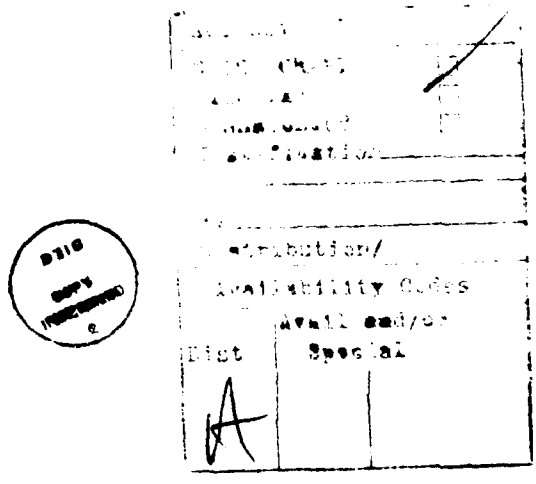

LIST OF FIGURES

LIST OF FIGURES (Concluded)

I. INTRODUCTION

Research areas in experimental mechanics have been greatly expanded since the introduction of the He-Ne laser in 1960. Initial engineering applications utilized holographic interferometry to measure surface deformations of opaque solids. Original applications suggested that the modern techniques in coherent optics would possibly change the method of measurement of strains and stresses; however, this has not been the case, although many engineering examples have been successfully demonstrated. Some of the authors' contributions are listed in references [1-7]. Although interference fringes are well defined in holography, difficulties exist because of the sensitivity of the measurements which require vibration isolation and the ability to separate displacement components from a single hologram. Thus, holography has not developed as a general technique of experiemtal stress analysis, and still remains a technique of the specialist.

Objects illuminated with coherent light are observed to have a granular appearance known as the laser speckle effect. The details of this structure do not resemble the microscopic character of the surface, but rather appear to be random in nature. This effect is described in terms of the interference of the microscopic nature of the surface when illuminated with a laser. Interference of the dephased, but coherent, waves results in this speckle effect [8]. This effect has provided for a method of surface displacement measurements known as laser speckle interferometry, which does not require vibration isolation. In addition, this technique is a direct measure of in-plane displacements; thus, the separation of components is accomplished easily [7]. All coherent optical methods are a measure of surface displacements or its derivatives on the boundary of a solid; thus, the need still exists to calculate stresses and strains at any desired point in a three-dimensional body from the surface data.

The concept of speckle was first applied to optical systems; however, modern applications reveal that the speckle effect occurs in many areas of physics and engineering [8-10] as a result of the ubiquitous character of the random interference phenomenon. Examples of analogies to the laser speckle effect include radar astronomy, synthetic aperture radar, recent developments in ultrasonic holography, and theory of spectral analysis of random processes. Goodman [8] illustrates that the basic concepts of speckle are much broader than originally envisioned with the laser, and that the results apply to all related phenomena, so long as the basic statistical assumptions are satisfied. Because of these parallels, the results of the laser speckle effects in optics suggest the possibility of an acoustical speckle effect utilizing ultrasonics. The direct extension of substituting an ultrasonic wave for coherent light is an obvious one, since it was first performed in the acoustical holography. An acoustical speckle interferometry study has been demonstrated to be a direct measure of object motion [11,12], which closely parallels laser speckle interferometry. The particular significance of the ultrasonics is the fact that subsurface scattering points can be recorded and correlated to measure acoustical signals. Thus, acoustical speckle interferometry has the potential to measure displacements of interior points in opaque solids. The extension to include measurements of deformable bodies will result in a technique to measure directly strains at interior points in otherwise opaque solids.

II. ELASTODYNAMIC THEORY

Acoustical speckle interferometry is based locally on the elastodynamic response of solids subjected to ultrasonic waves. The basic theory will be governed by the following set of field equations for a homogeneous isotropic medium.

The stress tensor $\sigma_{ij}(\underset{\sim}{X})$ is related to the gradient of displacements by the following equation

$$\sigma_{ij} = \lambda U_{k,k}\,\delta_{ij} + \mu(U_{i,j} + U_{j,i}) \tag{1}$$

where the comma denotes partial differentiation and λ and μ are the Lame's constants.

Balance of linear momentum yields the following equation of motion written in terms of displacement gradients.

$$\mu\, U_{i,jj} + (\lambda + \mu)\, U_{j,ii} + \rho\ddot{U} = f_i \tag{2}$$

where ρ is the mass density and f_i are the components of the body force per unit volume.

Solution of the equations of motion (2) must satisfy appropriate boundary conditions. The displacement boundary value problem assumes a knowledge of displacements on the entire surface S.

$$U_i(\underset{\sim}{X}) = \bar{U}_i(\underset{\sim}{X}) \tag{3}$$

when $\underset{\sim}{X}$ denotes the orthogonal coordinates X_1, X_2, X_3 and $\bar{U}_i$ are known values of the surface displacements. The traction boundary value problem is

$$t_i(\underset{\sim}{X}) = \sigma_{ij}\,\eta_j = \bar{t}_i(\underset{\sim}{X}) \tag{4}$$

when the vector function $\bar{t}_i(\underset{\sim}{X})$ is prescribed for $\underset{\sim}{X}\varepsilon S$. Unit vector η_j is the outward normal vector for the body P.

As an initial approximation to the local response of an elastic body to an ultrasonic wave, consider a plane displacement wave propagating with phase velocity C in a direction described by a propagation vector $\vec{p}$ as [13].

$$\vec{U} = \vec{A}de^{i\eta} \tag{5}$$

where

$$\eta = K(\vec{X}\cdot\vec{p} - ct)$$

Equation (5) describes a plane harmonic wave with $\vec{X}\cdot\vec{P}$ = constant describing a plane normal to the propagation vector $\vec{p}$.

Two types of plane harmonic waves described by Equation (5) exist which are solutions to Equation (2). Waves of the type where $\vec{d} = \pm\vec{p}$ are called

longitudinal waves and the phase velocity is denoted as C_L. Waves of this type, where $\vec{d} \cdot \vec{p} = 0$, are called transverse waves, and the phase velocity for this type of wave is denoted as C_T.

Substitution of Equation (5) into Equation (1) yields the following form for the components of the stress tensor.

$$\sigma_{ij} = \left[\lambda \delta ij (d_\ell p_\ell) + \mu(d_i\, p_j + d_j p_i)\right] ikAe^{i\eta} \tag{6}$$

when the summation convention is employed.

The presence of a subsurface layer or disconunity generally produces a change in the wave propagating in a medium. Acoustical speckle interferometry utilizes the reflection, refraction, and mode conversion of incident elastic waves at the interface of two elastic media as a basic description of the transmission and reflection of elastic waves. Consider initially two joined elastic half-spaces, as illustrated in Figure 1. An incident longitudinal wave, denoted as a p-wave, is incident on the boundary of the two elastic half-spaces. At the interface, boundary conditions and conditions of continuity will result in both reflection and refraction of longitudinal and transverse waves from an incident p-wave. The notation and description of the waves will be the same as described in reference [13] and repeated here for completeness of discussion. Unit propagation vectors are illustrated in Figure 1, with material properties of the incident medium denoted as λ, ρ, μ. Material properties of the refracted medium are labeled λ^B, μ^B, ρ^B. Superscripts, p^n, on the propagation vectors are used to describe the reflected and refracted waves as given in the following equations.

Incident Longitudinal wave (p-wave), n = 0.

The incident P-wave will be described by the unit propagation vector $\vec{p}^o$, when

$$p^o = \cos\theta_o \vec{i}_1 + \sin\theta_o \vec{i}_2 \tag{7-a}$$

Displacement vector is described as $\vec{d}^o = \vec{p}^o$; therefore

$$\vec{U}^o = A_o \left[\cos\theta\ \vec{i}_1 + \sin\theta_o \vec{i}_2\right] e^{i\eta_o} \tag{7-b}$$

and

$$\eta = K_o \left[X_1 \cos\theta_o + X_2 \sin\theta_o - C_o t\right] \tag{7-c}$$

Stress components for the incident p-wave are calculated from Equation (6) and are

$$\tau_{21}^o = ik_o (\lambda + 2\mu \cos^2\theta_o) A_o e^{i\eta_o} \tag{8-a}$$

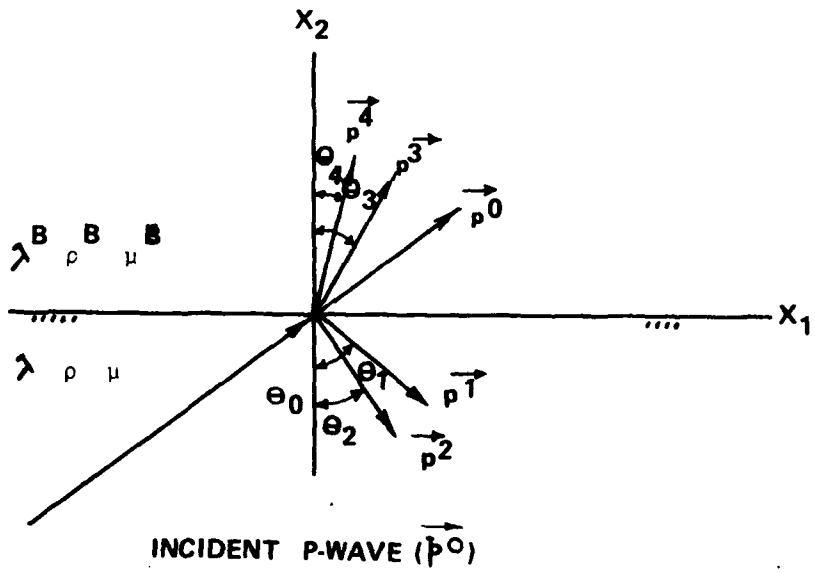

Figure 1. Incident, reflected and refracted elastic waves at the boundary of joined half spaces.

$$\tau_{22}^{o} = 2ik_o \mu \sin\Theta_o \cos\Theta_o A_o e^{i\eta_o} \quad (8\text{-b})$$

Reflected longitudinal wave, n = 1.

The reflected p-wave is described by the unit propagation vector as

$$\vec{p}^{1} = \sin\Theta_1 \vec{i}_1 - \cos\Theta_1 \vec{i}_2 \quad (9\text{-a})$$

Displacement vector is $\vec{d}^{1} = \vec{p}^{1}$

$$\vec{U}^{1} = A_1 \left[\sin\Theta_1 \vec{i}_1 - \cos\Theta_1 \vec{i}_2\right] e^{i\eta_1} \quad (9\text{-b})$$

where

$$\eta_1 = k_1 \left[X_1 \sin\Theta_1 - X_2 \cos\Theta_1 - C_1 t\right] \quad (9\text{-c})$$

Stresses for this wave are

$$\tau_{21}^{1} = ik_o \mu \sin 2\Theta_1 A_1 e^{i\eta_1} \quad (10\text{-a})$$

$$\tau_{22}^{1} = i k_1 \left[\lambda + 2\mu \cos^2\Theta_1\right] A_1 e^{i\eta_1} \quad (10\text{-b})$$

Reflected transverse wave (sv-wave), n = 2.

Propagation vector, displacement vector and stress components are given by the following equations.

$$\vec{p}^{2} = \sin\Theta_2 \vec{i}_1 - \cos\Theta_2 \vec{i}_2 \quad (11\text{-a})$$

The description of a transverse vertical wave is given by $\vec{d}_2 = \vec{i}_3 + \vec{p}_2$, which yields the following form for the displacement vector.

$$\vec{U}^{2} = A_2 \left[\cos\Theta_2 \vec{i}_1 - \sin\Theta_2 \vec{i}_2\right] e^{i\eta_2} \quad (11\text{-b})$$

$$\eta_2 = k_2 \left[X_1 \sin\Theta_1 - X_2 \cos\Theta_2 - C_2 t\right] \quad (11\text{-c})$$

$$\tau_{21}^{2} = -\frac{ik_o C_L \mu}{C_T} \cos 2\Theta_2 A_2 e^{i\eta_2} \quad (12\text{-a})$$

$$\tau_{22}^{2} = -ik_2 \mu \sin 2\Theta_2 A_2 e^{i\eta_2} \quad (12\text{-b})$$

Refracted longitudinal wave, n = 3.

$$\vec{p}^3 = \sin\theta^3\vec{i}_1 + \cos\theta_3\vec{i}_2 \tag{13-a}$$

$$\vec{U}^3 = A_3\left[\sin\theta_3\vec{i}_1 + \cos\theta_3\vec{i}_2\right]e^{i\eta_3} \tag{13-b}$$

$$\eta_3 = K_3\left[X_1\sin\theta_3 + \cos\theta_3 - C_3t\right] \tag{13-c}$$

$$\tau_{21}^3 = \frac{iK_oC_L}{C_L^B}\mu B\sin 2\theta_3A_3\,e^{i\eta_3} \tag{14-a}$$

$$\tau_{22}^3 = ik_3\left[\lambda^B + 2\mu^B\cos^2\theta_3\right]A_3\,e^{i\eta_3} \tag{14-b}$$

Refracted transverse wave, n = 4.

The transverse vertical wave in the refracted medium is described by $\vec{d}^3 = \vec{i}_3 X p$ where

$$\vec{p}^4 = \sin\theta_4\vec{i}_1 + \cos\theta_4\vec{i}_2 \tag{15-a}$$

$$\vec{U}^4 = A_4\left[-\cos\theta_4\vec{i}_1 + \sin\theta_4\vec{i}_2\right]e^{i\eta_4} \tag{15-b}$$

$$\eta_4 = K_4\left[X_1\sin\theta_4 + X_2\cos\theta_4 - C_{4_t}\right] \tag{15-c}$$

$$\tau_{21}^4 = iK_4\mu^B\cos 2\theta_4A_4e^{i\eta_4} \tag{16-a}$$

$$\tau_{22}^4 = iK_4\mu^B\sin 2\theta_4A_4e^{i\eta_4} \tag{16-b}$$

At the interface, a condition of perfect contact will be assumed and the displacement and traction vector at the interface $X_2 = 0$ must be continuous for all X_1 and t.

$$\vec{U}^0 + \vec{U}^1 + \vec{U}^2 = \vec{U}^3 + \vec{U}^4 \tag{17-a}$$

$$\vec{t}^0 + \vec{t}^1 + \vec{t}^2 = \vec{t}^3 + \vec{t}^4 \tag{17-b}$$

These equations written in component notation are

$$U_i^0 + U_i^1 + U_i^2 = U_i^3 + U_i^4 \tag{18-a}$$

$$\overset{1}{\tau}_{2_i} + \overset{1}{\tau}_{2_i} + \overset{2}{\tau}_{2_i} = \overset{3}{\tau}_{2_i} + \overset{4}{\tau}_{2_i} \qquad i = 1,2 \qquad (18\text{-b})$$

Equations (7-c, 9-c, 11-c, 13-c) require that boundary conditions are satisfied for all X_1 and t yields the following.

$$K_0 \sin\Theta_0 = K_1 \sin\Theta_1 = K_2 \sin\Theta_2 = K_3 \sin\Theta_3 = K_4 \sin\Theta_4 \qquad (19\text{-a})$$

$$K_0 C_L = K_1 C_L = K_2 C_T = K_3 C_L^B = K_4 C_T^B \qquad (19\text{-b})$$

Equations (17-a) and (7-b, 9-b, 11-b, 13-b) yield the following conditions on continuity of displacements at the interface.

$$A_0 \sin\Theta_0 + A_1 \sin\Theta_1 + A_2 \cos\Theta_2 = A_3 \sin\Theta_3 - A_4 \cos\Theta_4 \qquad (20)$$

$$A_0 \cos\Theta_0 - A_1 \cos\Theta_1 + A_2 \sin\Theta_2 = A_3 \cos\Theta_3 + A_4 \sin\Theta_4 \qquad (21)$$

Equation (18-b), coupled with Equations (8, 10, 12, 14), yield the following conditions for conditions on the components of the stress tensor at the interface.

$$\mu A_0 \sin 2\Theta_0 - \mu A_1 \sin 2\Theta_1 - \mu A_2 \frac{CL}{CT} \cos 2\Theta_2 = \frac{C_L}{C_L^B} \mu^B A_3 \sin 2\Theta_3 - A_4 \frac{C_L}{C_T^B} \mu^B \cos 2\Theta_4 \qquad (22)$$

$$K_0 \left[\lambda + 2\mu \cos^2\Theta_0\right] A_0 + K_1 \left[\lambda + 2\mu \cos^2\Theta_1\right] A_1 - K_2\mu \sin 2\Theta_2 A_2 = K_3 \left[\lambda^B + 2\mu^B \cos^2\Theta_3\right] A_3 + K_4 \mu^B \sin 2\Theta_4 A_4 \qquad (23)$$

Equations (20-23) can be put in a matrix form amenable to computation for a system of n layered media.

$$[A][X] = [B] \tag{24}$$

where

$$[A] = \begin{bmatrix} -\sin\theta_1 & -\cos\theta_2 & \sin\theta_3 & -\cos\theta_4 \\ \cos\theta_1 & -\sin\theta_2 & \cos\theta_3 & \sin\theta_4 \\ \mu\sin 2\theta_1 & \mu\frac{C_L}{C_T}\cos 2\theta_2 & \frac{C_L}{C_L}\mu^B\sin 2\theta_3 & -\frac{C_L}{C_T}\mu^B\cos 2\theta_4 \\ -(\lambda+2\mu\cos^2\theta_1) & \frac{C_L}{C_T}\mu\sin 2\theta_2 & \frac{C_L}{C_L}\lambda^B+2\mu^B\cos^2\theta_3 & \frac{C_L}{C_T}\mu^B\sin 2\theta_4 \end{bmatrix}$$

$$[X] = \begin{bmatrix} A_1/A_0 \\ A_2/A_0 \\ A_3/A_0 \\ A_4/A_0 \end{bmatrix}$$

$$[B] = \begin{bmatrix} \sin\theta_0 \\ \cos\theta_0 \\ \mu\sin 2\theta_0 \\ \lambda + 2\mu\cos\theta_0 \end{bmatrix}$$

Equation (24) forms the solution for the amplitude ratios A_i/A_0 for the reflection and refraction of an incident p-wave of two perfectly joined half-spaces. For a system of n-layers, Equations (19) and (24) can be utilized to determine the propagation and energy partition at the boundary of each layer.

Some special cases of the interfaces are of primary importance for problems in acoustical speckle interferometry. A liquid-solid boundary usually forms the initial interface, and a solid-liquid boundary forms the last boundary interface for a solid immersed in a liquid. In addition, a subsurface layer from a practical point forms a boundary of an elastic body with air, which is the condition of a subsurface void. At this interface, the refraction of elastic waves will be neglected; therefore, only the reflection of elastic waves at a free surface will be considered. Since these special cases are of particular importance in acoustical interferometry, they will be examined in some detail.

A. Liquid-Solid Boundary

Suppose that the medium comprised of the incident p-wave is liquid and the refracting medium is an elastic solid. For this condition, the reflected SV-wave is zero; therefore, the boundary conditions reduce to the following form.

$$U_i^0 + U_i^1 = U_i^3 + U_i^4 \qquad (i = 1,2) \tag{25}$$

$$\tau_{22}^0 + \tau_{22}^1 = \tau_{22}^3 + \tau_{22}^4 \tag{26}$$

$$\tau_{21}^3 + \tau_{21}^4 = 0$$

Equations (25) and (26) are solved for the amplitude ratios Ai/A0, and are displayed in matrix form for computation.

$$\begin{bmatrix} -\sin\Theta_1 & \sin\Theta_3 & -\cos\Theta_4 \\ \cos\Theta_1 & \cos\Theta_3 & \sin\Theta_4 \\ -\lambda & \frac{C_L}{C_L^B}\left[\lambda^B + 2\mu^B\cos^2\Theta_3\right] & \frac{C_L}{C_L^B}\mu^B\sin 2\Theta_4 \end{bmatrix} \begin{bmatrix} A_1/A_0 \\ A_3/A_0 \\ A_4/A_0 \end{bmatrix} = \begin{bmatrix} \sin\Theta_0 \\ \cos\Theta_0 \\ \lambda \end{bmatrix} \tag{27}$$

B. Solid-Liquid Boundary

The boundary between the two layers is comprised of an elastic solid reflecting medium and a liquid refracting medium. The p-wave ($\vec{p}^0$) represents the incident wave and the transmitted sv-wave is zero. Boundary conditions reduce to the following.

$$U_i^0 + U_i^1 + U_i^2 = U_i^4 \qquad (i = 1,2) \tag{28}$$

$$\tau_{22}^0 + \tau_{22}^1 + \tau_{22}^2 = \tau_{22}^4 \tag{29}$$

$$\tau_{21}^0 + \tau_{21}^1 + \tau_{21}^2 = 0 \tag{30}$$

Equations (28, 29) are solved, and in matrix notations are written in terms of Ai/A0 as

$$\begin{bmatrix} -\sin\Theta_1 & -\cos\Theta_2 & \sin\Theta_3 \\ \cos\Theta_1 & -\sin\Theta_2 & \cos\Theta_3 \\ \left[\lambda + 2\mu\cos^2\Theta_1\right] & \frac{C_L}{C_T}\mu\sin 2\Theta_2 & \frac{C_L}{C_L}\lambda^B \end{bmatrix} \cdot \begin{bmatrix} A_1/A_0 \\ A_2/A_0 \\ A_3/A_0 \end{bmatrix} = \begin{bmatrix} \sin\Theta_0 \\ \cos\Theta_0 \\ \lambda + 2\mu\cos^2\Theta_0 \end{bmatrix} \tag{31}$$

C. Free Boundary

At a free surface, the following boundary conditions are satisfied for the stress components.

$$\overset{0}{\tau}_{2_i} + \overset{1}{\tau}_{2_i} + \overset{2}{\tau}_{2_i} = 0 \qquad i = 1,2 \tag{32}$$

Solution of Equation (32) in terms of the amplitude ratios are [13]

$$\frac{A_1}{A_0} = \frac{\sin 2\Theta_0 \sin 2\Theta_2 - K^2 \cos^2 2\Theta_2}{\sin 2\Theta_0 \sin 2\Theta_2 + K^2 \cos^2 2\Theta_2} \tag{33-a}$$

$$\frac{A_1}{A_0} = \frac{2K \sin 2\Theta_0 \cos 2\Theta_2}{\sin 2\Theta_0 \sin 2\Theta_2 + K^2 \cos^2 2\Theta_2} \tag{33-b}$$

where

$$K = \left[\frac{2(1-\nu)}{1-2\nu}\right]^{\frac{1}{2}}$$

III. NUMERICAL RESULTS

The numerical solution for a layered elastic half space immersed in a liquid medium involves the solution of Equations (24), (27), and (31) for the amplitude ratios A_1/A_0, A_2/A_0, A_3/A_0, and A_4/A_0. Equation (27) is utilized to determine the amplitude ratios at a liquid-solid boundary for an incident p-wave in the liquid. At each solid boundary, Equation (24) is used to calculate the amplitude ratios. At the solid-liquid boundary, amplitude ratios are calculated by Equation (31). Thus, for a multiple-layered medium, these equations are repeatedly applied for the number of interfaces.

As an illustration of the liquid-solid boundary equation, consider an incident p-wave in water at a steel interface for various angles of incidence Θ_0. As expected, an incident p-wave gives rise to a reflected p-wave and transmitted p-waves and sv-waves in the solid. Equation (27) was solved numerically for the following data.

λ steel = 16.42×10^6 psi

ρ steel = 0.284 lbm/in^3

μ steel = 11.6×10^6 psi

β water = 0.318×10^6 psi

ρ water = 0.0361 lbm/in^3

Amplitude ratios for various values of the incident angle Θ_0 are given in Figure 2.

An incident p-wave in a solid at a water interface gives rise to both reflected p-waves and sv-waves and a transmitted p-wave. Equation (31) is used to calculate the amplitude ratios at this boundary and in Figure 3 the amplitude ratios are shown versus the angle of incidence Θ_0.

A solid elastic half space for an incident p-wave in one solid gives rise to both reflected and refracted p-waves and sv-waves in each solid. The amplitude ratios for this boundary are calculated from Equation (24). As an illustration of this solution procedure an incident p-wave in steel at a steel aluminum boundary is used as data for the calculation of the amplitude ratios for various angles of incidence Θ_0. Data for the aluminum are shown in Figure 4.

λ Aluminum = 7.42×10^6 psi

μ Aluminum = 4.00×10^6 psi

ρ Aluminum = 0.100 lbm/in^3

An example problem of a two-layered elastic half space immersed in water is chosen to illustrate the solution procedure for the layered medium problem. Geometry for this example is shown in Figure 5, and only reflected and refracted p-waves at each interface are shown in this illustration; however, sv-waves exist at each solid boundary. The particular significance of the p-waves is in the application of acoustical speckle interferometry to object motion measurements in layered media. Reference [12] illustrates that the p-waves are amenable to object motion measurement; therefore, this discussion will be restricted to p-wave propagation. Consider an incident p-wave in water at interface 1 which is a liquid-solid boundary. Solid 1 is taken to be steel with the same properties for the liquid-solid example. Superscripts refer to the particular wave component, as discussed in the previous section, and subscripts refer to each boundary. A transmitted p-wave at boundary 1 will become an incident p-wave at boundary 2 and incident angle $\Theta_2^0 = \Theta_1^3$. For the two-layer elastic half space, the incident waves at each boundary are listed in the following:

Boundary 1: $\vec{P}_1^0 = \vec{P}^0$, $\Theta_1^0 = \Theta^0$

Boundary 2: $\vec{P}_2^0 = \vec{P}_1^3$, $\Theta_2^0 = \Theta_1^3$

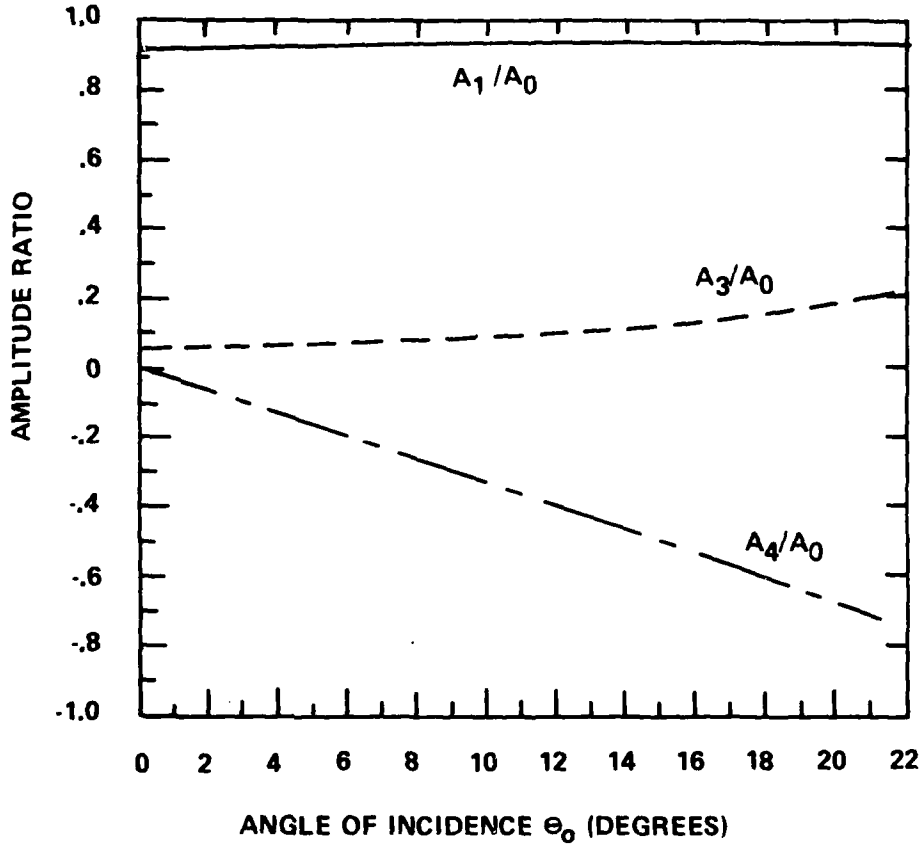

Figure 2. Amplitude ratio of a water steel interface for an incident p-wave in water.

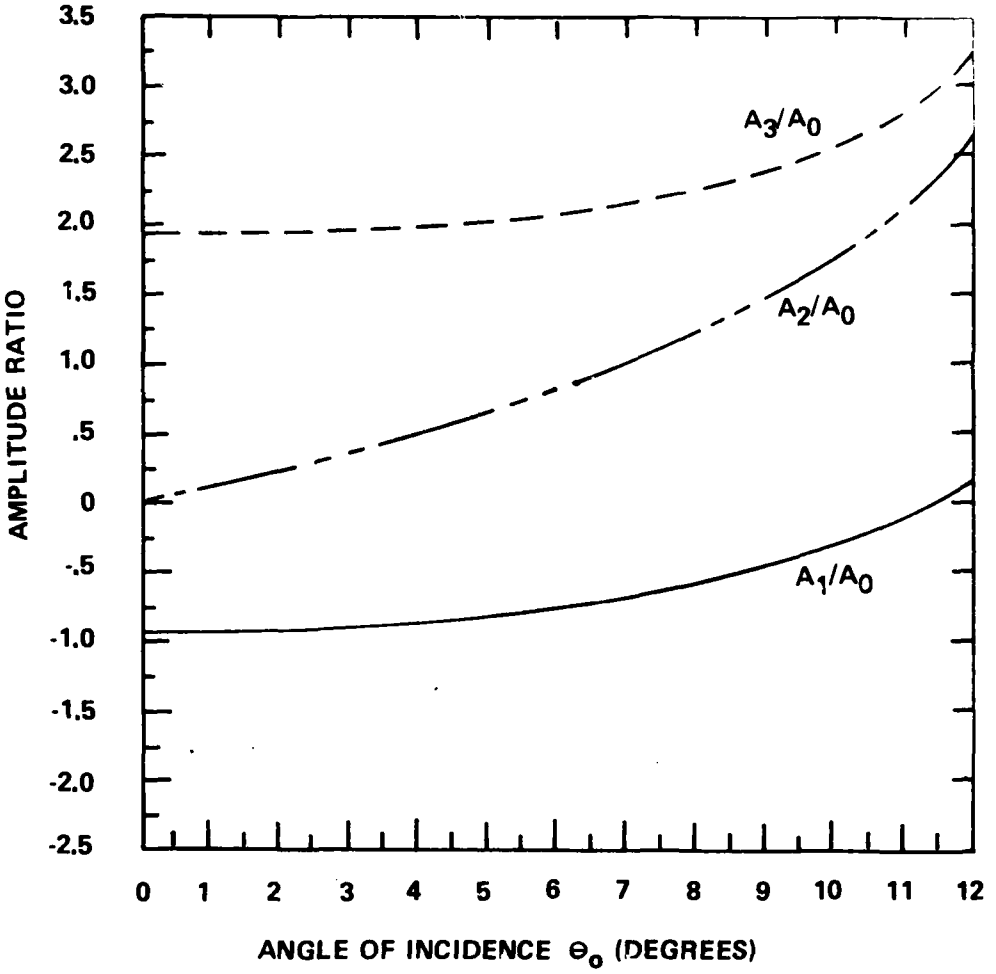

Figure 3. Amplitude ratio of a steel water interface for an incident p-wave in steel.

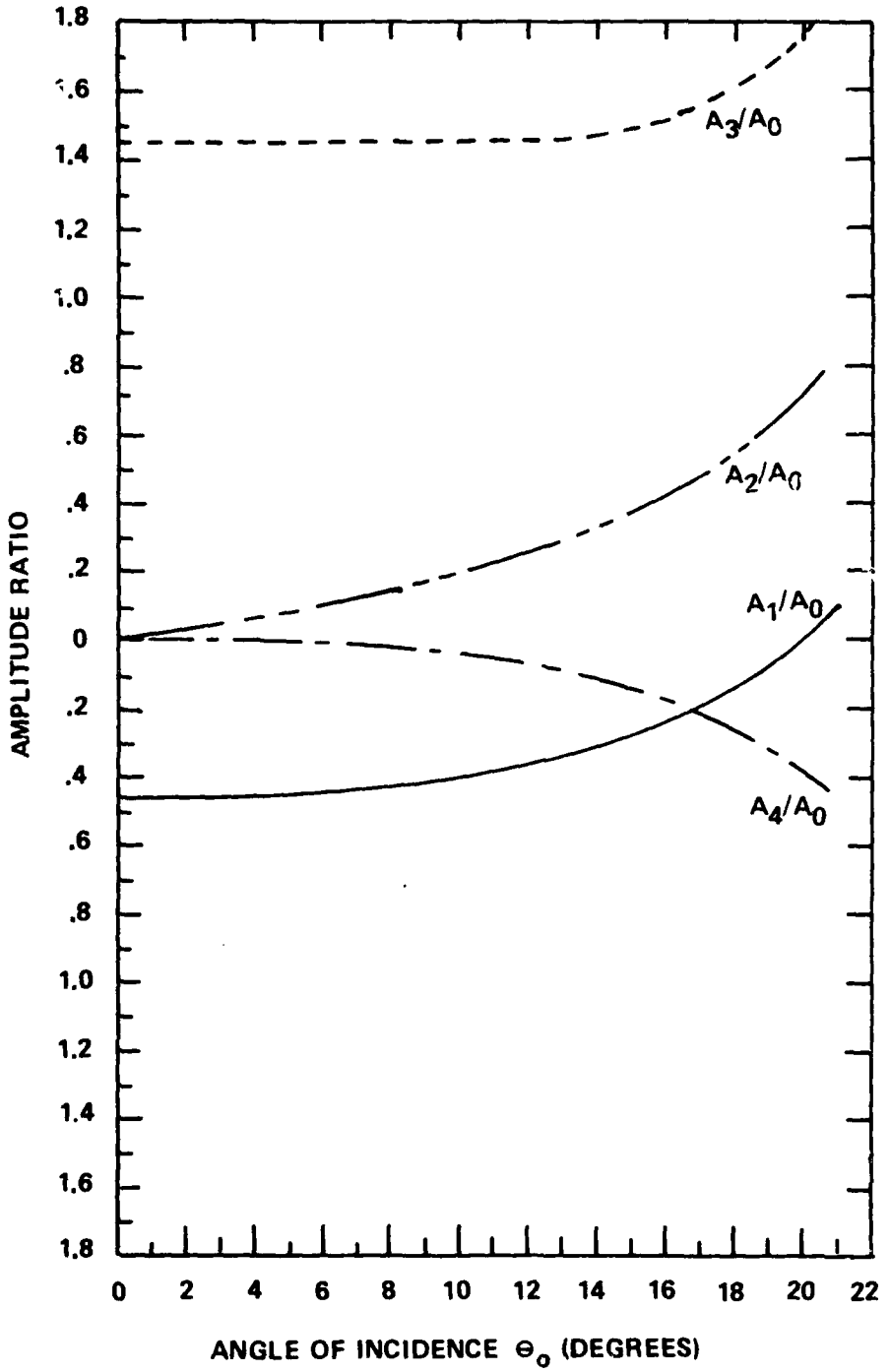

Figure 4. Amplitude ratio of an aluminum steel elastic half space for an incident p-wave in aluminum.

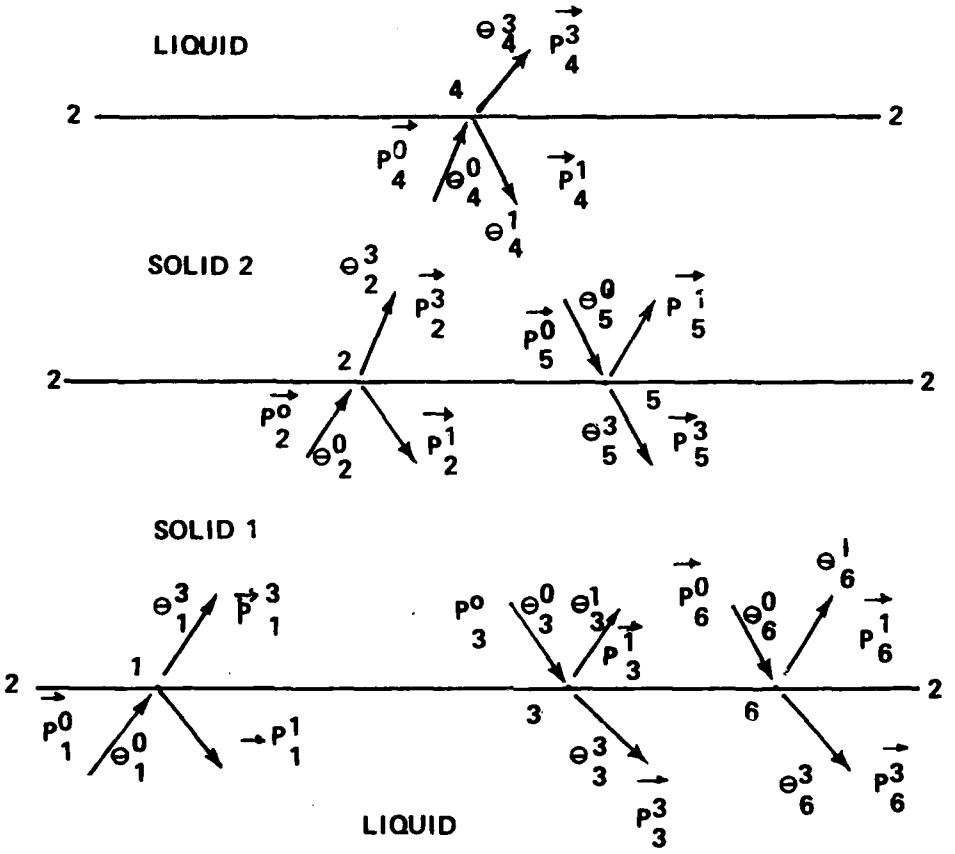

Figure 5. Reflection and refraction of p-waves in a layered medium for an incident p-wave in the liquid medium.

Boundary 3: $\vec{P}_3^0 = \vec{P}_2^1$, $\Theta_3^0 = \Theta_2^0$

Boundary 4: $\vec{P}_4^0 = \vec{P}_2^3$, $\Theta_4^0 = \Theta_2^3$

Boundary 5: $\vec{P}_0^5 = \vec{P}_4^1$, $\Theta_5^1 = \Theta_4^1$

Boundary 6: $\vec{P}_6^0 = \vec{P}_5^3$, $\Theta_6^0 = \Theta_5^3$

Amplitude ratios at each interface for an initial incidence angle $\Theta^0 = 0^0$ are listed in the following for the two-layer elastic half space. The computer program for these calculations is listed in Appendix A.

Liquid-Solid 1 Boundary 1

$A_1/A_0 = 0.93810$

$A_3/A_0 = 0.061905$

$A_4/A_0 = 0.00$

Solid 1-Solid 2 Boundary 2

$A_1/A_0 = -0.45965$

$A_2/A_0 = 0.00$

$A_3/A_0 = 1.4597$

$A_4/A_0 = 0.00$

Solid 1-Liquid Boundary 3

$A_1/A_0 = -0.93809$

$A_2/A_0 = 0.00$

$A_3/A_0 = 1.9381$

Solid 2-Liquid Boundary 4

$A_1/A_0 = -0.8411$

$A_2/A_0 = 0.00$

$A_3/A_0 = 1.8411$

Solid 2-Solid 1 Boundary 5

$A_1/A_0 = 0.45965$

$A_2/A_0 = 0.00$

$A_3/A_0 = 0.54035$

$A_4/A_0 = 0.00$

Solid 1-Liquid Boundary 6

$A_1/A_0 = -0.93809$

$A_2/A_0 = 0.00$

$A_3/A_0 = 1.9381$

Amplitude ratios at each interface for an initial incidence angle $\Theta^0 = 20^0$ are listed as follows:

Liquid-Solid Boundary 1

$A_1/A_0 = 0.92684$

$A_3/A_0 = 0.17302$

$A_4/A_0 = 0.65243$

Solid 1-Solid 1 Boundary 2

$A_1/A_0 = 0.44433$

$A_2/A_0 = 0.09316$

$A_3/A_0 = 1.4611$

$A_4/A_0 = 0.017700$

Solid 1- Liquid Boundary 3

$A_1/A_0 = 0.81650$

$A_2/A_0 = 0.69193$

$A_3/A_0 = 2.0430$

Solid 2- Liquid Boundary 4

$A_1/A_0 = 0.72645$

$A_2/A_0 = 0.65056$

$A_3/A_0 = 1.9423$

Solid 2- Solid 1 Boundary 5

$A_1/A_0 = 0.44651$

$A_2/A_0 = 0.08059$

$A_3/A_0 = 0.53946$

$A_4/A_0 = 0.0077461$

Solid 1- Liquid Boundary 6

$A_1/A_0 = -0.81650$

$A_2/A_0 = 0.69193$

$A_3/A_0 = 0.02430$

IV. ACOUSTICAL SPECKLE INTERFEROMETRY

As a tool of quantitative nondestructive testing of materials, the spectral analysis of ultrasonic pulses in elastic solids has attracted wide attention in recent years. Krautkrämer [14] suggested in 1959 that measurement of the pulse shape could be used to determine the size and orientation of flaws in materials. Methods for determining the spectral content of broad-band ultrasonic pulses reflected and scattered in materials were subsequently developed by Gericke [15]. In his pioneering work, he showed that

the spectral content of pulses propagating in steel specimens was greatly dependent on the material's microstructure. In later work [16], he investigated the spectral content of echoes from cylindrical cavities oriented perpendicular and parallel to the direction of wave propagation. From these experiments he concluded that it might be feasible to use ultrasonic-spectroscopy measurements in conjunction with normal pulse-echo techniques to determine not only the location of a defect, but also its shape. Brown [17] has reviewed some results obtained by Lloyd [18] on the spectral response of various conical and flat-topped cylinders, which could be explained qualitatively in terms of the cylinder's dimensions and geometry. Sachse [19] has reported an experimental investigation of the spectral analysis of wide-band ultrasonic pulses as scattered by a circular, cylindrical, fluid-filled cavity in an elastic solid. It was shown that either the diameter of the cavity or the wave speed of the fluid can be determined from the time record of the scattered pulses. Furthermore, an empirical formula was developed to relate the diameter and the wave speed to the intervals between the minima or maxima of the power spectra. The author concluded that the method of ultrasonic spectroscopy which are originated by Gerick can be used to detect the dimensions and mechanical properties of flaws and impurities inside elastic solids.

Theories of the scattering of acoustic waves have been extensively devleoped since the fundamental work of Lord Rayleigh [20]. A review of the existing theories as well as some numerical results of scattered waves in elastic solids have been published in the monograph by Pao and Mow [21]. The case of a circular, cylindrical cavity inside an elastic solid was investigated in detail by White [22]. He measured amplitudes and arrival times of plane harmonic waves with long duration, using standard ultrasonic techniques. His measured angular distributions of the scattered wave amplitudes for both incident longitudinal and shear waves agreed very well with his theoretical analysis.

The interaction of sound waves and pulses with solid cylinders immersed in a fluid has been of interest in underwater acoustics for some time. Most extensively studied has been the scattering of pulses incident normal to the axis of the cylinder. In 1967, Goodman, Bunney, and Marshall [23] reported the existence of a Rayleigh-type circumferential wave propagating around a solid cylinder. Later, Neubauer [24-26] reported the results of experiments in which pulses were used to study the propagation of the circumferential waves on aluminum cylinders immersed in water. In 1969, Bunney, Goodman, and Marshall [27] also reported observation of the Rayleigh-type wave. Several experiments of the scattering of broad-band ultrasonic pulses by cylindrical inclusions in elastic solids have been performed by Sachse and Chian [28] and Bifulco and Sachse [29]. The inclusions were fluids or solids whose wave speed was less than that of the solid matrix material. It was shown that in a non-destructive testing application, the size and wave speed of the inclusion could be determined from measurements of the arrival times of various scattered pulses. In a recent work [30] measurements are reported of the arrival times of broad-band ultrasonic pulses scattered by a circular, cylindrical solid inclusion imbedded in a matrix whose longitudinal wave speed is lower than that of the scatter.

In many instances in practice, it is highly desirable to obtain an accurate and rapid measure of the stress in a structural member. Ultrasonics

offers a great tool for the realization of a system capable of performing this task. Ultrasonic-pulse spectroscopy measurements has been used to measure the stress-induced interference effects between two shear waves propagating in uniaxially deformed specimens of aluminum [31]. This technique shows considerable promise as a means for measuring and monitoring the applied stresses in materials.

Ensminger [32] documents many modern applications dealing with topics such as thickness measurements, inspection of metals and non-metals and the determination of bond integrity. Ultrasonic inspection is further being extended to tissue examinations and bone scans in the medical field [33].

As an experimental nor-destructive stress analysis, the polarized transverse ultrasonic waves have provided a new method of measurements which is christened the acoustoelasticity. Similar to the photoelastic effect, the velocity of the transverse soundwaves traversing a stressed elastic solid is not a constant as it would be in an isotropic solid. The velocity depends on the direction of the particle motion (polarization), the direction of wave propagation, and the state of stress. With the recent advancement of ultrasonic techniques, one can generate, transmit and detect plane polarized ultrasounds. Therefore, stress-induced acoustical birefringence can be measured. As in photoelasticity, the difference of propagation velocities in shear waves polarized in principal stress directions is proportional to the principal-stress differences in the plane-stress state. Thus, this technique is a nondestructive test method and determines stresses by ultrasonic shear waves which do not require a transparent plastic model [34-36].

Plastic deformation in crystalline solids by means of high-frequency stress wave propagations has been studied by a number of investigators [37,38]. The study of the relation between the propagation of ultrasonic waves and plastic deformation in single crystals has been discussed in detail. Specifically, changes in attenuation and velocity of ultrasonic waves have been measured as a function of plastic strain during the deformation process. These techniques have also been applied to the investigation of some aspects of strain hardening mechanisms [39].

Knowledge and control of the transmission and reflection of ultrasonic waves in layered media is an important basic problem in underwater acoustics. The problem of transmission of sound at oblique incident angles through a solid multilayer system of plane parallel plates was treated by Thompson [40], Brekhovskikh [41], and others. The most detailed solution of the multilayer problem is by Shaw and Bugl [42], whose theoretical approach was directed toward the investigation of conditions under which interface waves may be generated. In a recent work [43], the wave equation was solved to determine the transmission and reflection coefficients for plane waves at oblique incidence on a system of n layers of plane parallel plates.

Acoustic holography is the newest branch in acousting imaging technology. It is directly comparable with optical holography in the phenomenological sense, because to make a hologram it is necessary that the two beams of radiation used have the ability to interfere with one another. Acoustic holography underwent very rapid development during the last few years, and simulated the general field of acoustic imaging through the introduction of novel techniques for visualizing acoustic excitation. In contrast to optical holography, which

has sometimes been described as a solution looking for a problem, acoustical holography was from the outset developed for a specific purpose. This purpose is that of all acoustical probing systems, namely, detecting, locating, and imaging a structure immersed in a medium opaque to electromagnetic radiation. This description encompasses a variety of specific problems, such as non-destructive testing, medical imaging, oil exploration, and underwater imaging.

A recent development in laser technology, referred to as speckle interferometry, has provided for a new technique in experimental mechanics to measure surface displacements of deformed solids. Basically this method records the laser intensity variation across the surface of an object due to the random interference of the microscopic character of the illuminated surface. Figure 6 illustrates the basic method for recording a double exposure laser speckle photograph. A high resolution photographic film records the granular pattern on the film plane of a camera. If the object is displaced from a reference configuration, the speckles are mapped to a new location on the film plane corresponding to the object motion. Data analysis consists of pointwise filtering as illustrated schematically in Figure 7. This method of data analysis assumes a constant value of displacement within the small area of illumination, and the resulting interference pattern is obtained by taking optically the Fourier transform of the amplitude transmission function of the photographic transparency. Interference fringes are therefore a direct measure of local object motion within the area of illumination. The discrete global response of the body is obtained by pointwire filtering of many small areas of the photograph transparency.

Because the speckle effect is statistical in nature and the basic concepts occur in many areas of physics and engineering, the previously developed techniques in optics suggest a parallel development in ultrasonics. In a recent work [11,12] a basic theory of one-dimensional pulse-echo and continuous wave acoustical speckle interferometry was developed. This method utilized the statistical concepts of speckle and one-dimensional correlation of reference and displaced signals to determine object motion of subsurface scattering layers. This study established the feasibility of the acoustical speckle concept for object motion measurements.

V. BASIC THEORY OF DISPLACEMENT MEASUREMENTS UTILIZING ULTRASONICS

This section presents the geometrical concepts of displacement functions of a continuum and the correlation of a reference and deformed ultrasonic signal as a measure of object motion. The basic problem may be described in the following way: given the measured ultrasonic global response of signals before and after deformation, it is then required to calculate the local object displacement vector from the global reference and deformed configurations of a body. Thus the basic problem is geometrical in nature and initially is not concerned with the external forces necessary to cause the geometrical deformation.

Let the position of the points in a continuum in the initial (unstrained state) be given with respect ot the coordinates X_1, X_2, X_3, as illustrated in Figure 8. The body is deformed with respect to the unstrained coordinates and points are displaced to new coordinates denoted as X_1', X_2', X_3' (Figure 8).

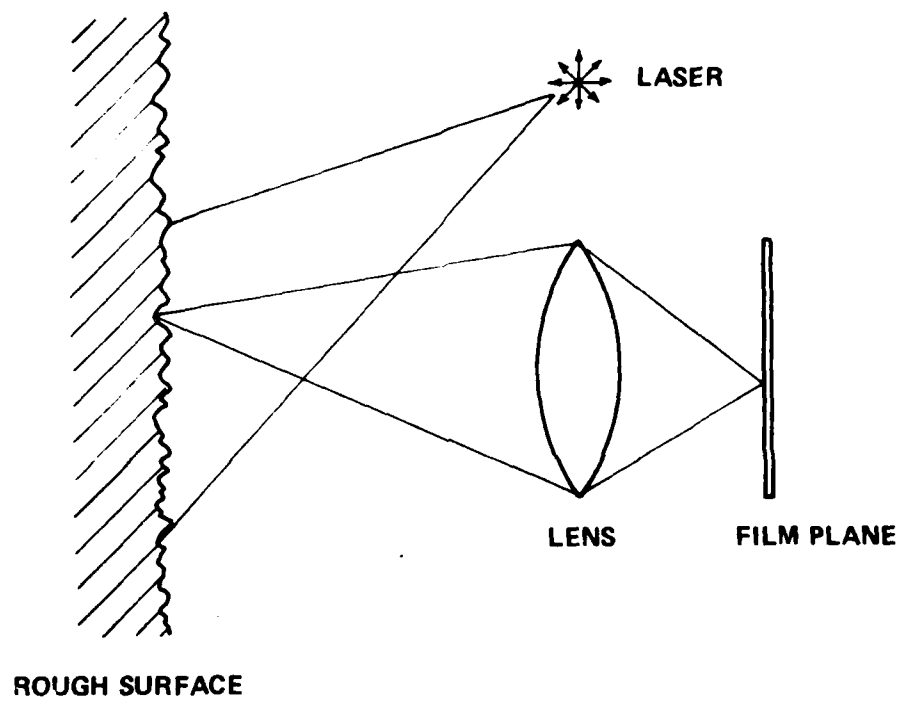

Figure 6. Formation of a laser speckle photograph.

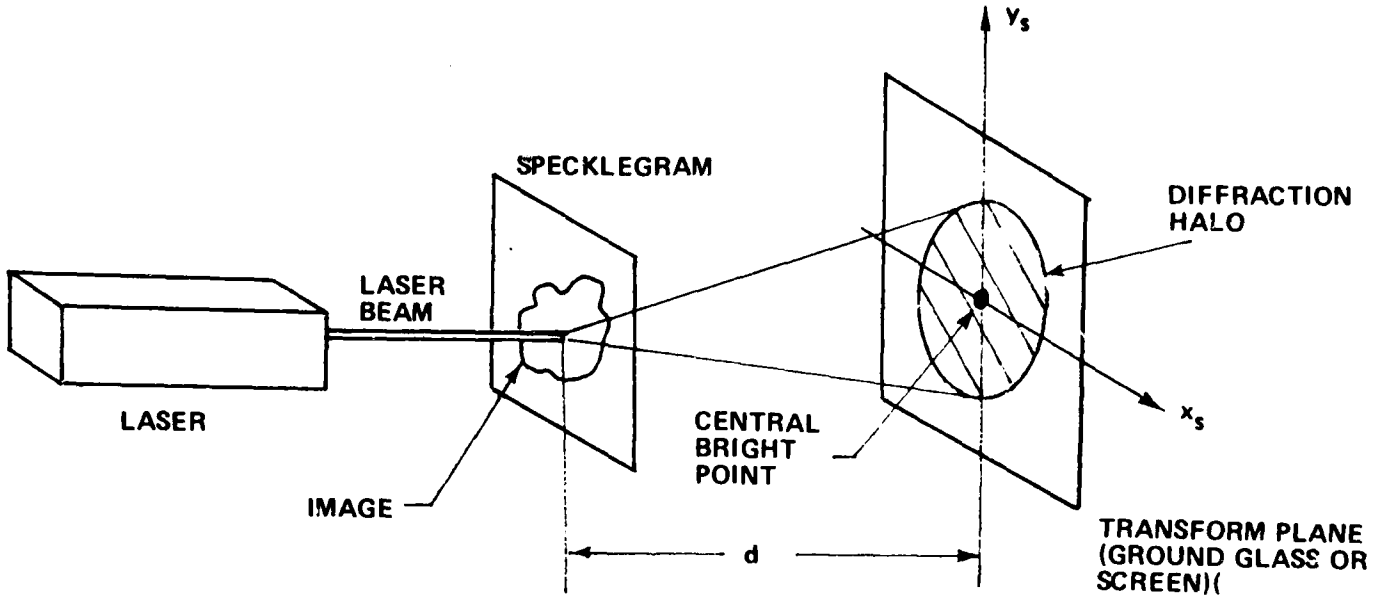

Figure 7. Data analysis for pointwise filtering in in-plane measurements.

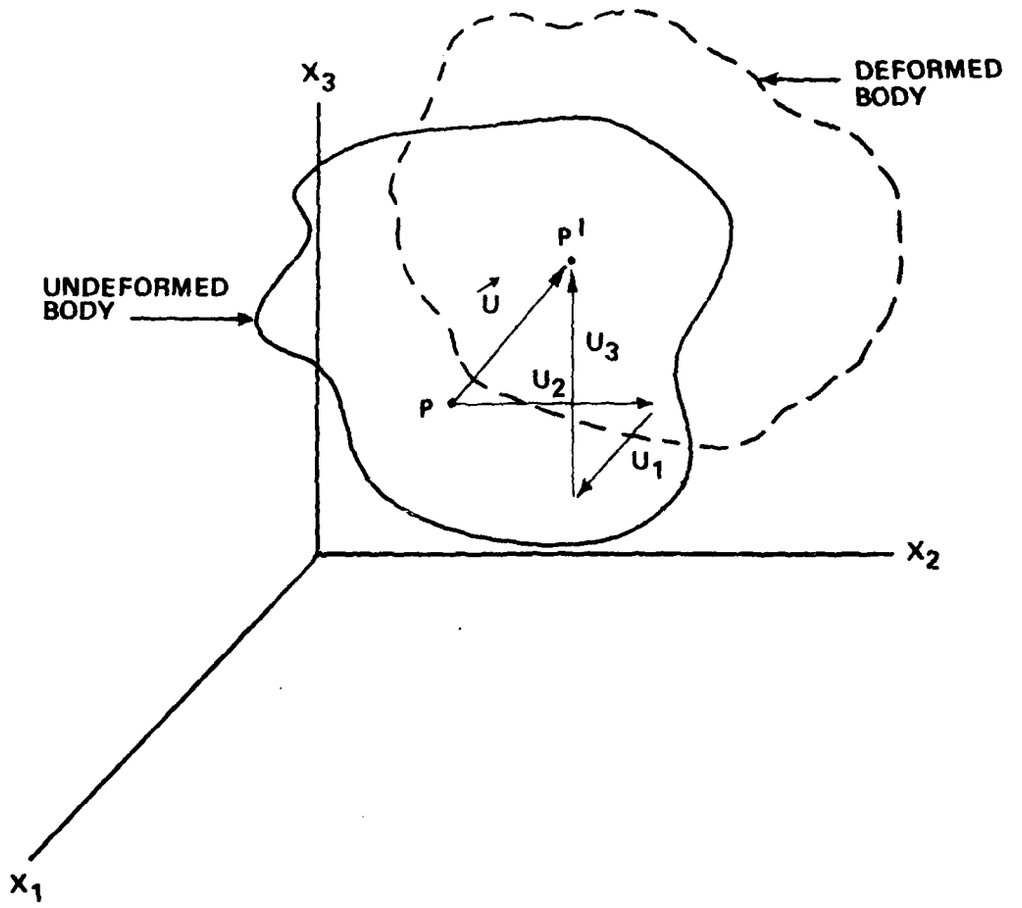

Figure 8. Displacement components of a deformed body.

The coordinates of an arbitrary point in the deformed configuration are expressed in terms of the original coordinates by the following equation.

$$X_i' = X_i + U_i(X_1, X_2, X_3, t) \tag{34}$$

where U_i are called displacement components and are taken to be continuous functions of the original coordinates X_1, X_2, X_3. Thus, in general, the displacement functions vary from point to point in a deformed body.

Suppose a continuous mode or pulse echo ultrasonic scan is made of a rough scattering surface with reference area M as illustrated in Figure 9. The field reflected from the scattering surface at the plane of the receiving transducer in a plane immediately adjacent to that surface is described by a complex function $\alpha(\xi,\eta)$, which represents a reflected p-wave or SV-wave from an incident p-wave in an elastic solid. The complex field $P(\underset{\sim}{X})$ where $\underset{\sim}{X} = (X_1,X_2)$ denotes the ordered pair of numbers in the plane of the receiving transducer which is parallel to (ξ,η) and represents the amplitude of the reference signal, which is the field of interest from the acoustical signal. Details of both pulse echo and continuous mode scanning techniques of scattering surfaces are described in reference [11,12].

Now suppose that the receiving transducer is returned to the original position and the scattering surface is displaced from its reference configuration. A complex field $P(\underset{\sim}{X}')$ represents the amplitude of the received signal where the coordinates $\underset{\sim}{X}' = X_1',X_2'$ are parallel to the plane (ξ,η). If the displacements functions in Equation (34) are substituted into the representation of the displaced signal, the special form reduces to the following:

$$P(\underset{\sim}{X}') = P(X_1 + U_1, X_2 + U_2) \tag{35}$$

where the received signal is assumed to be a function of the coordinates parallel to the plane of the scattering surface. The reference and displaced signals are illustrated in Figure 10.

The problem now becomes one of correlating the signals $P(\underset{\sim}{X})$ and $P(\underset{\sim}{X}')$ to measure the local displacement components U_1 and U_2. The basis for this measurement is the autocorrelation function of the two signals which is given in the following equation:

$$C(U_1,U_2) = \int_M P(X_1,X_2)\, P(X_1 + U_1,X_2 + U_2)\, dX_1 dX_2 \tag{36}$$

The one-dimensional correlation of continuous mode scanning for a rigid deformation is discussed in reference [12]. This study demonstrated that Equation (36) forms the basic concept for object motion measurement of subsurface acoustic scattering layers which agrees with the statistical relationships in laser speckle interferometry.

Although Equation (36) has been demonstrated to be a measure of object motion, some limitations are imposed on the applications because the

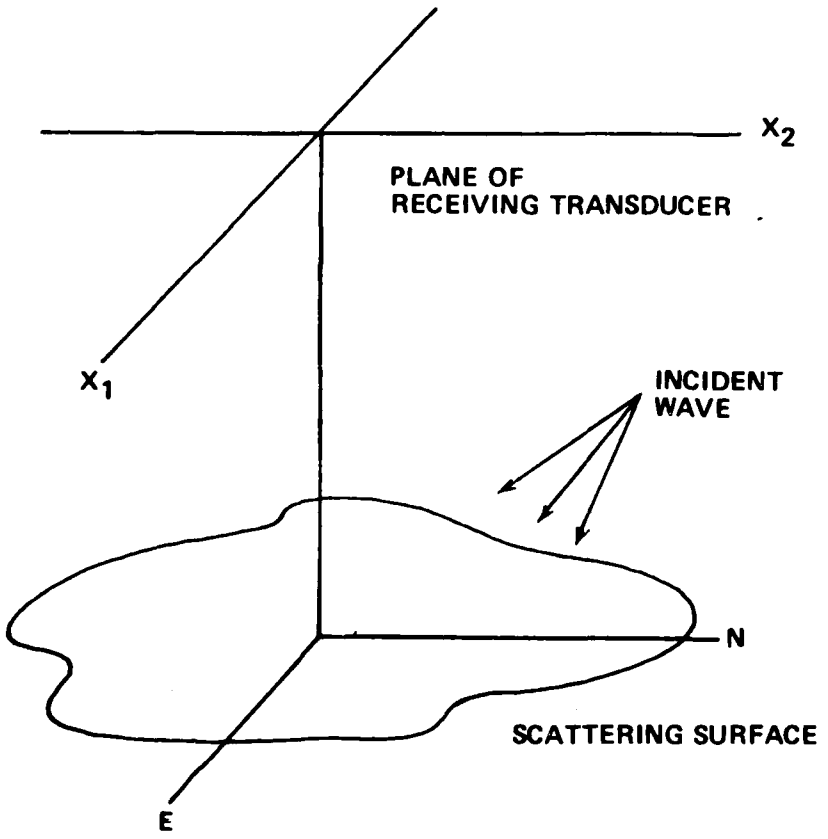

Figure 9. Free space geometry for acoustical speckle.

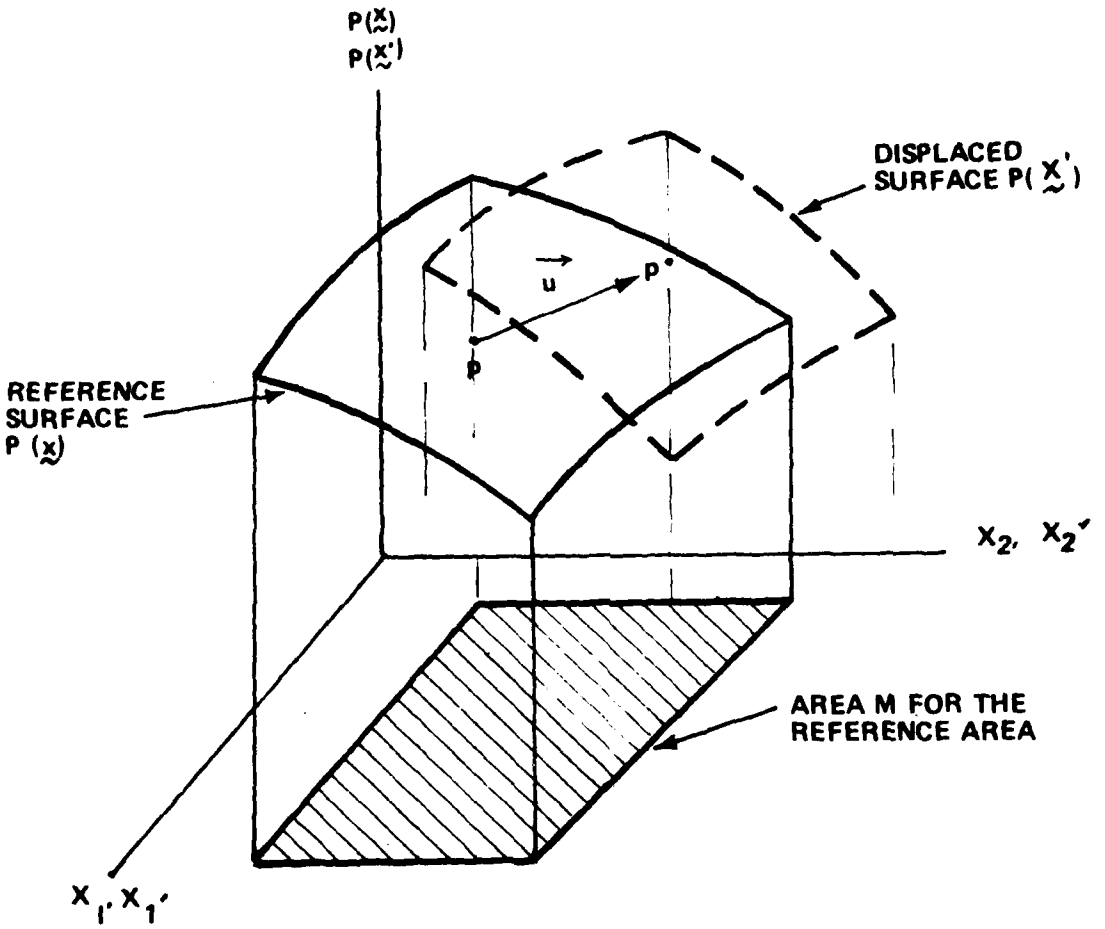

Figure 10. Reference and deformed surface for correlation of acoustical signals.

displacement functions U_1 and U_2 are, in general, continuous functions of the initial coordinates (X_1, X_2) and are the unknown quantities to be determined. If the displaced surface is just a uniform translation in the X_1, X_2 directions, then U_1, U_2 are constant and the application of Equation (36) is straightforward; however, in the presence of a deformed surface, U_1 and U_2 cannot be interpreted in terms of a global uniform translation. The basic approach used in computing the correlation of $P(\underset{\sim}{X})$ and $P(\underset{\sim}{X}')$ is to assume the basic theory of data analysis in pointwise filtering used in single beam laser speckle interferometry (Figure 11). Object motion displacements are obtained by passing a laser beam through a small area of a double exposed transparency which contains both the reference and deformed images. Interference fringes are observed as intensity of the light amplitude in the transform plane. This analysis utilizes the shift theorem which restricts the displacement components to be constant within the area of illumination. Practical applications for a He-Ne laser restricts the area to be a circular region approximately 2 mm in diameter.

This restriction in optics suggests the following approach in acoustical speckle interferometry. Let the reference scan be recorded over some reference area M in the X_1, X_2 plane, as illustrated in Figure 11. Suppose that within some small neighborhood of a point $P_o \in P(\underset{\sim}{X}')$ the displacement is assumed to be uniform. The acoustical signal corresponds to a small neighborhood of the point $P_o \in P(\underset{\sim}{X})$. Therefore the Equation (36) can now be used in the form

$$\Delta C(U_1, U_2) = \int_M \Delta P(X_1, X_2) \Delta P(X_1 + U_1, X_2 + U_2)\, dX_1 dX_2 \qquad (37)$$

where $\Delta P(\underset{\sim}{X})$ and $\Delta P(\underset{\sim}{X}')$ correspond to a small surface surrounding the points of interest. The correct values of U_1, U_2 corresponding to the object motion displacement will result in a maximum value of the correlation function $\Delta C(U_1, U_2)$. This correlation procedure corresponds to the data analysis at pointwise filtering in optics and thus completes the analysis of the displacement of a point. The procedure to determine the discrete displacement values will follow the procedure in optics as discussed in reference [7].

A discussion of the cross-correlation peak should include the effects of deformation on the local accuracy of the correlation function. This problem in local deformation of an object is similar to the problem of image correlation with geometric distortion on the accuracy of image restoration [44]. Basically, the image restoration is investigated for distortions represented by an affine transformation of image coordinates, which is an offset plus scaling and rotation of each image coordinate axis [45-47]. The image analysis assumes a fixed geometric distortion and then a proper choice of integration area in the cross-correlation can be optimized for minimum local error. Geometric distortion for deformable bodies is generally unknown; therefore, this represents the inverse problem to image registration. A discussion of this problem will include the restrictions and assumptions in the linear theory of elasticity and an example problem will be chosen to illustrate the effects.

Let a point P be displaced to a point P', and point Q displaced to Q'. The displacement of point Q can be expanded in a linear Taylor's series as expressed in the following form.

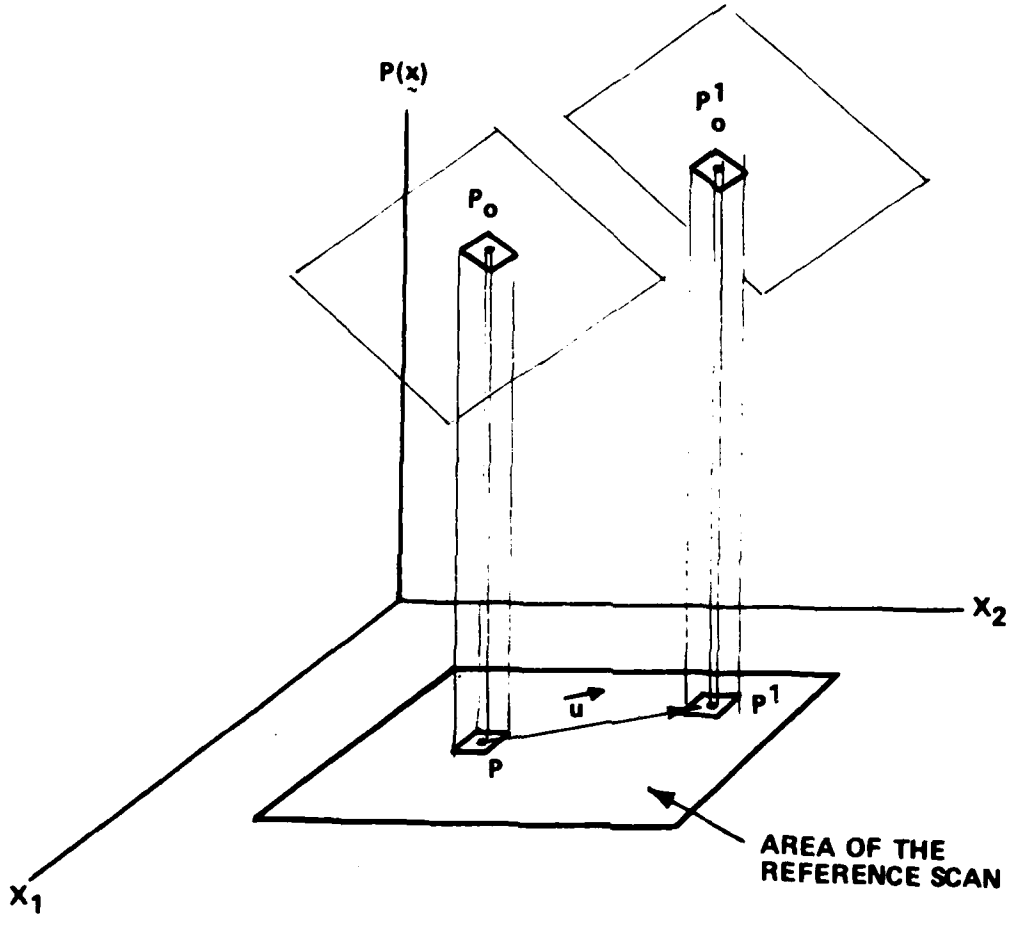

Figure 11. Reference and displaced subsets of the original and displaced surfaces.

$$U_1 \mid Q = U_1 \mid P + \frac{\partial U_1}{\partial X_1} \Delta X_1 + \frac{\partial U_1}{\partial X_2} \Delta X_2 \tag{38}$$

$$U_2 \mid Q = U_2 \mid P + \frac{\partial U_2}{\partial X_1} \Delta X_1 + \frac{\partial U_2}{\partial X_2} \Delta X_2$$

Equation (38) can be expressed in terms of the infinitesimal strains and rotation components which results in the following expression [48].

$$U_1 \mid Q = U_1 \mid P + \Delta U_1 \tag{39}$$

$$U_2 \mid Q = U_2 \mid P + \Delta U_2$$

where

$$\Delta U_1 = \varepsilon_{11} \Delta X_1 + (\varepsilon_{12} - \omega_3)$$

$$\Delta U_2 = (\varepsilon_{12} + \omega_3)\Delta X_1 + \varepsilon_{22}\Delta X_2$$

The correlation function can now be put in the following form.

$$\Delta C(U_1 + \Delta U_1, U_2 + \Delta U_2) = \int \Delta P(X_1, X_2) \Delta P(X_1 + U_1 + \Delta U_1, X_2 + \Delta U_2) \, d_{X_1} d_{X_2} \tag{40}$$

Equation (40) has been demonstrated to be a measure of object motion, taking into consideration the restrictions and assumptions in the linear theory of elasticity; however, Equation (36) represents the general measure of object motion. In the presence of a largely deformed surface U_1 and U_2 can be interpreted in terms of a rigid body translation and rotation and normal and shear strains. Several numerical examples will be discussed in order to illustrate the application of numerical correlation in object motion measurements.

VI. NUMERICAL EXAMPLES AND CONCLUSIONS

Several numerical examples will be discussed to illustrate the application of the numerical correlation in object motion measurements. A reference signal $P(\underset{\sim}{X})$ corresponding to the undeformed scan is illustrated in Figure 12. A line along the X_1 axis is shown in Figure 13. The reference area M for all examples presented will comprise an array of 100×100 data points. The displaced signal $P(\underset{\sim}{X}')$ will be correlated with the reference signal for the specific cases of displacement components U_1 and U_2. A correlation computer program is listed in Appendix B.

For a case of uniform translation in the absence of geometrical distortion, some simplifications in the integration area M allowed for a considerable reduction in computer time. The procedure utilized was to perform the correlation over two orthogonal lines of data points which comprise a length where object motion is assumed to be uniform. In the examples discussed, the five data points for this interval were used. Figure 14 is a graphical display of three examples of uniform translation. Figure 15 shows the surface $P(\underset{\sim}{X}')$ for a uniform translation in the X_1, X_2 directions. In order to demonstrate the generality of the computer program, an example of non-uniform translation without geometric distortion is discussed. The displacement along a line $y = \sin x$ for $0 \leq x \leq \pi$ is chosen to illustrate non-uniform translation and the results are shown in Figure 16.

Several examples for the case of uniform and non-uniform translations in the presence of geometric distortion (deformation) were solved. The results illustrated that for infinitesimal deformation (linear elasticity), geometric distortion had no effect on the correlation between reference and deformed signal.

Several examples of large deformations on the correlation of reference and deformed signals were considered to determine the accuracy of Equation (40) for large strains. Figures 17 through 19 are examples of the deformed surface $P(\underset{\sim}{X}')$ corresponding to large strains without rigid body motion. A comparison of these surfaces with the reference surface, as illustrated in Figure 12, shows the effect of geometric distortion relative to the reference surface. In each example of large geometric distortion the correlation accuracy was the same as the cases considered for uniform translation and infinitesimal deformations.

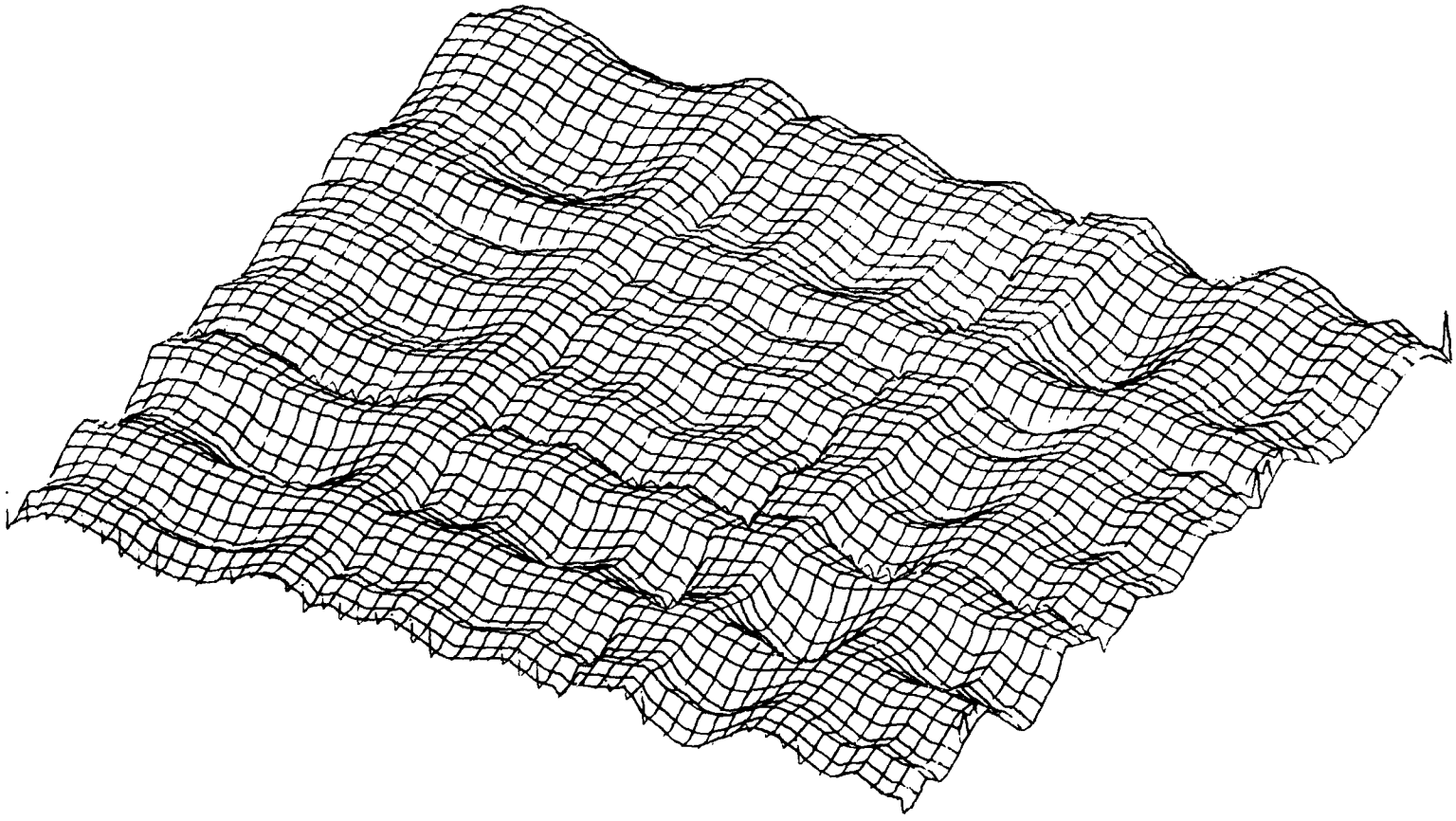

Figure 12. Three-dimensional acoustical surface corresponding to the reference signal P(X).

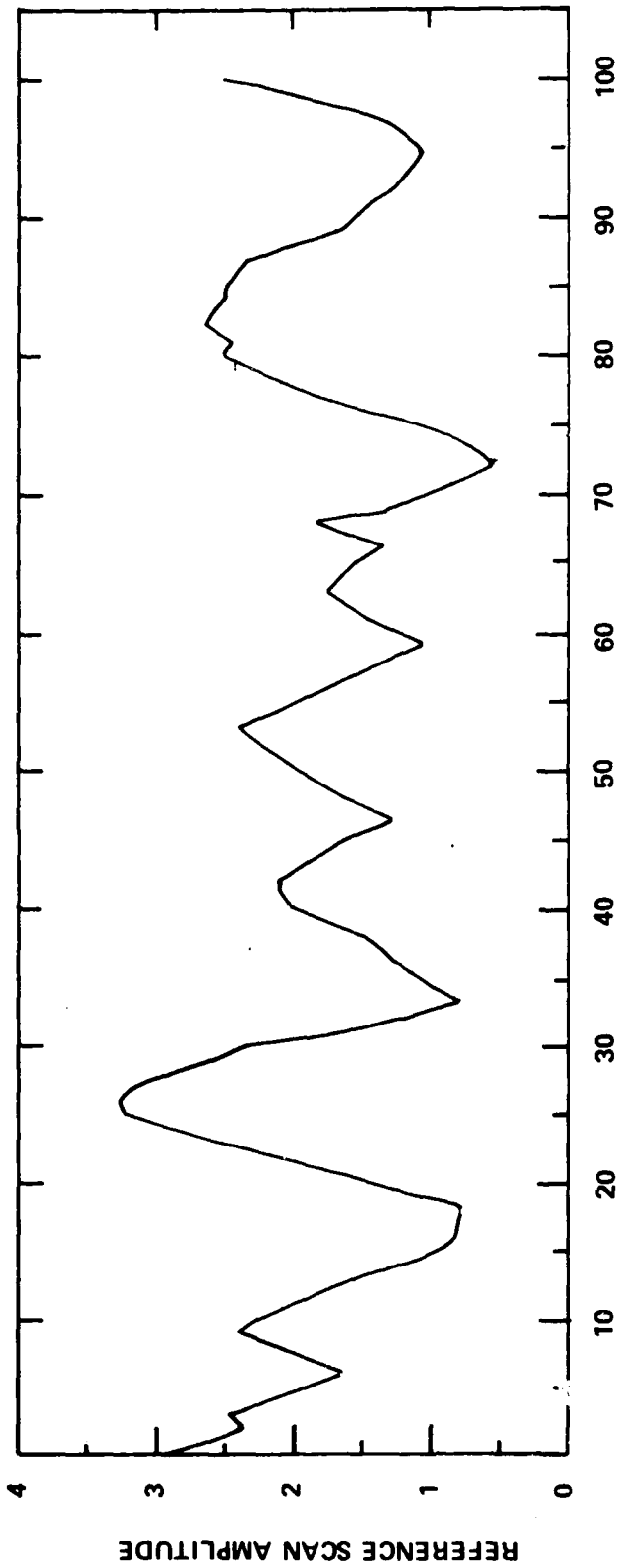

Figure 13. Reference signal along the X_1 axis $P(X_1,0)$.

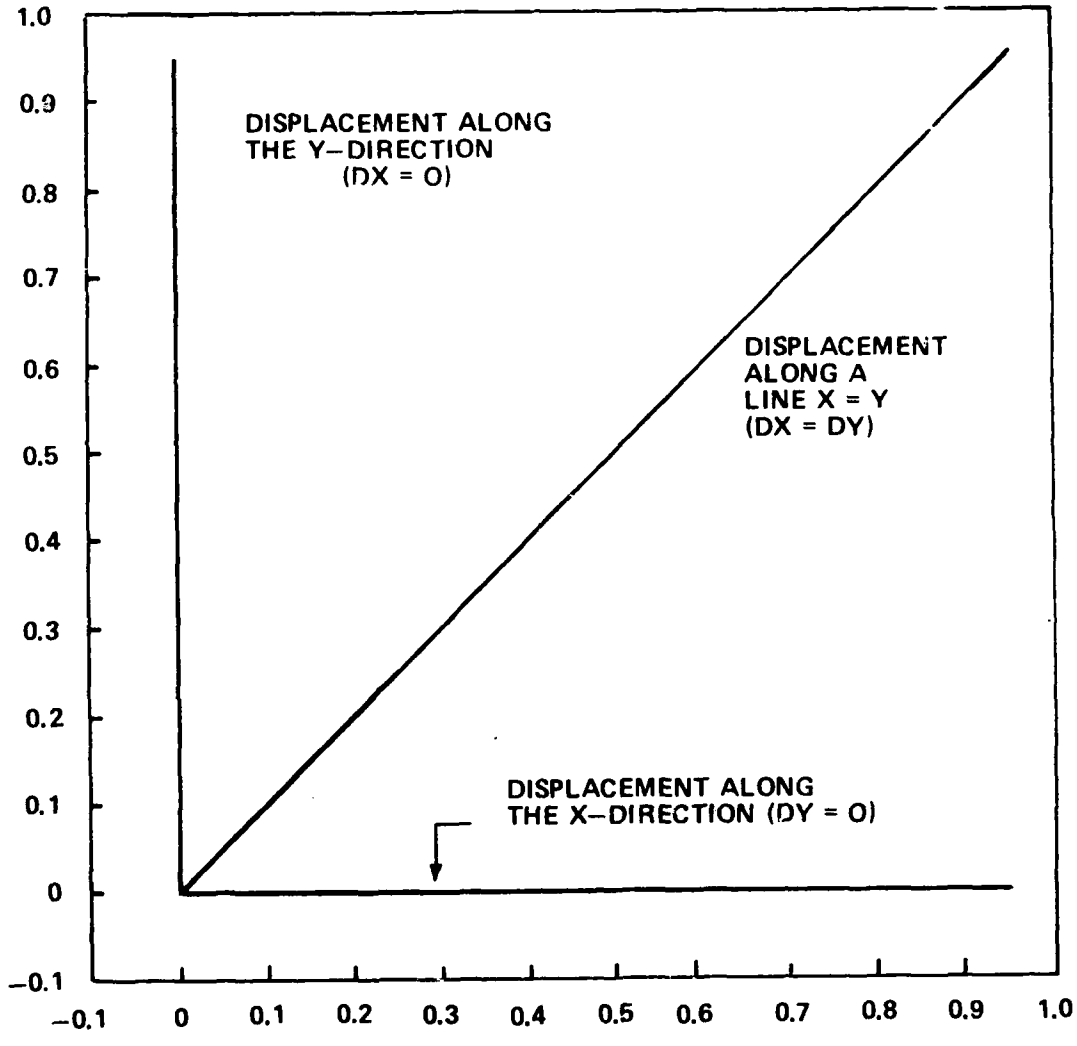

Figure 14. Uniform translation of a point P initially located at the origin.

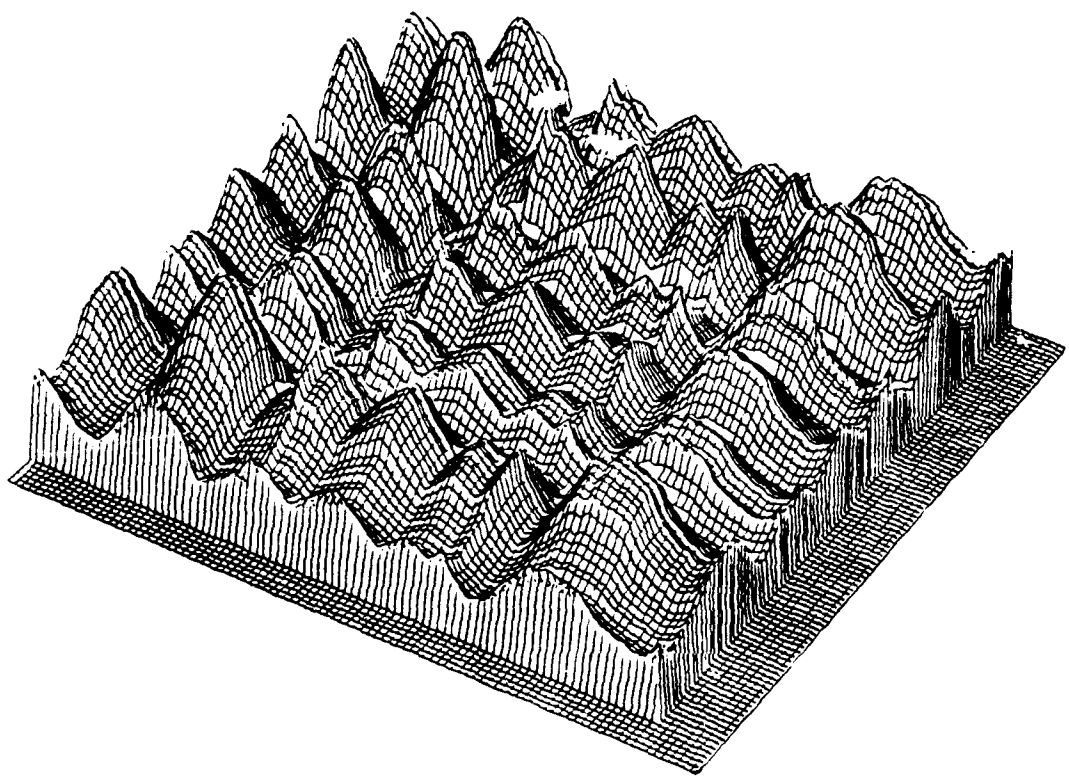

Figure 15. Acoustical surface corresponding to a uniform translation without geometric distortion -5 units X_1 direction -8 units in X_2 direction.

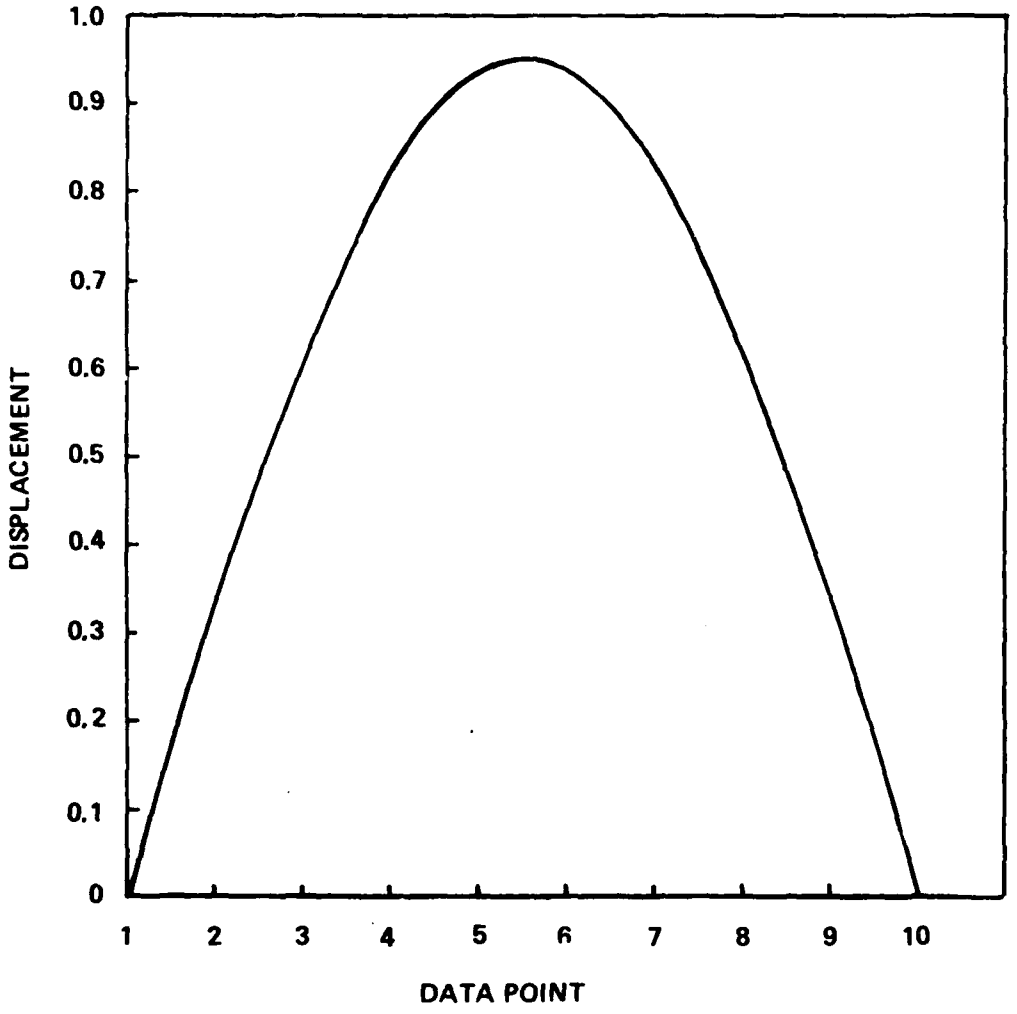

Figure 16. Non-uniform translation of a point P initially located at the origin.

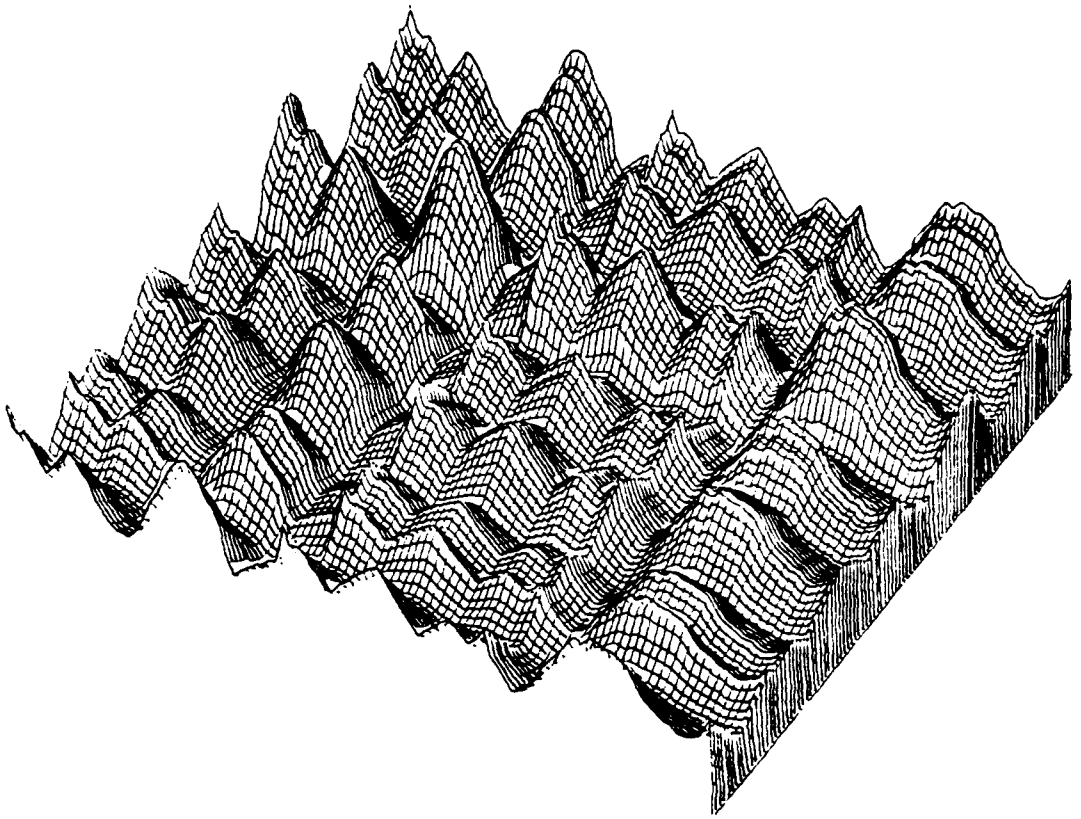

Figure 17. Acoustical surface $P(\underset{\sim}{X}')$ corresponding to a large strain $\varepsilon_{X_1} = 0.2$.

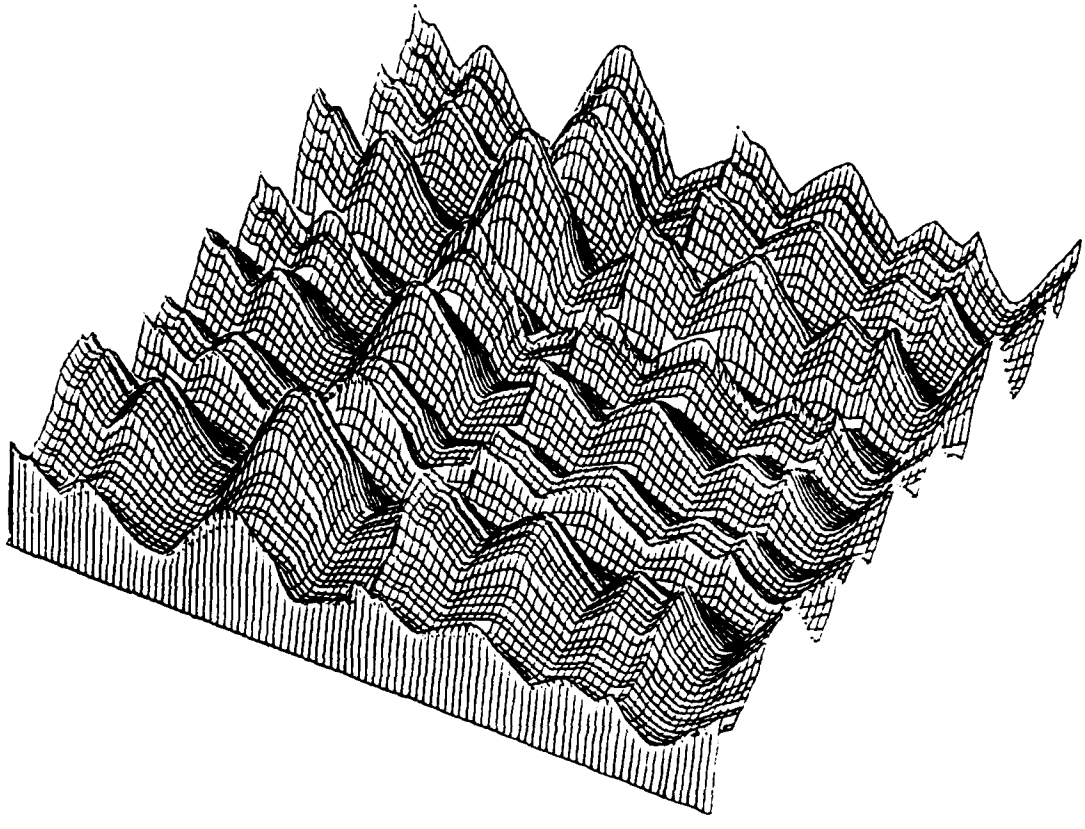

Figure 18. Acoustical surface $P(X')$ corresponding to a large strain $\epsilon_{X_2} \tilde{=} 0.2$.

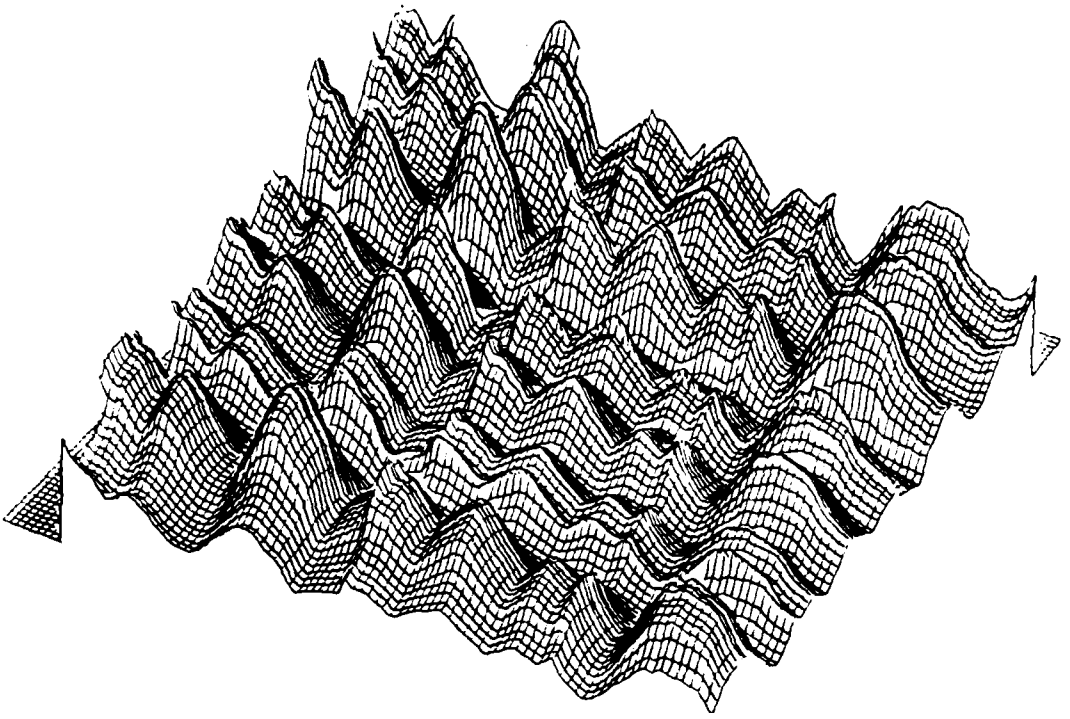

Figure 19. Acoustical surface $P(\underline{X}')$ corresponding to a large strain $\gamma_{X_1X_2} = 0.2$.

APPENDIX A

PROGRAM TO CALCULATE THE AMPLITUDE RATIO FOR A TWO-LAYER ELASTIC HALF SPACE IN A LIQUID

```
C     PROGRAM TO CALCULATE THE AMPLITUDE RATIO
C     FOR A TWO LAYER ELASTIC HALF SPACE IN A
C     LIQUID
C     EACH NUMBER CORRESPONDS TO AN INTERFACE
C
C     PROPERTIES OF THE LIQUID
      XLAL=318000.
      RHL=.0361
C     PROPERTIES OF SOLID 1
      XLA1=16420000.
      XM1=11600000.
      RH1=.284
C     PROPERTIES OF SOLID 2
      XLA2=7420000.
      XM2=4000000.
      RH2=.100
      CLL=4863.
      CL2=20341.
      CT2=10360.
      CL1=19348.
      CT1=10469.
C     LAYER 1---LIQUID-SOLID 1 INTERFACE
      THETA0=20.*3.1416/180.
      XLAM=XLAL
      RHO=RHL
      XLAMB=XLA1
      XMUB=XM1
      RHOB=RH1
      WRITE(5,3)
3     FORMAT(3X,'LIQUID-SOLID 1 INTERFACE')
      WRITE(5,4) THETA0
4     FORMAT(3X,'THETA0=',E12.5)
      CALL WASO(THETA0,XLAM,XMUB,XLAMB,RHO,RHOB)
      CL=CLL
      CLB=CL1
      CALL CRCSUB(CL,THETA0,CLB,YB)
      THET31=YB
      WRITE(5,5) THET31
5     FORMAT(3X,'THETA31=',E12.5)
C     LAYER 2---SOLID 1-SOLID 2 INTERFACE
      XLAM=XLA1
      XMU=XM1
      RHO=RH1
      XLAMB=XLA2
      XMUB=XM2
      RHOB=RH2
      THETA0=THET31
      WRITE(5,6)
6     FORMAT(3X,'SOLID 1-SOLID 2 INTERFACE')
      WRITE(5,7) THETA0
7     FORMAT(3X,'THETA0=',E12.5)
      CALL SOLID(THETA0,XMU,XLAM,XMUB,XLAMB,RHO,RHOB)
      CL=CL1
      CLB=CL2
```

```
      CALL CRCSUB(CL,THETA0,CLB,YC)
      THET32=YC
      WRITE(5,8) THET32
8     FORMAT(3X,'THETA32=',E12.5)
      CALL CRCSUB(CL,THETA0,CL,YA)
      THET12=YA
      WRITE(5,9) THET12
9     FORMAT(3X,'THETA12=',E12.5)
C     LAYER 3---SOLID 1-LIQUID INTERFACE
      XLAM=XLA1
      XMU=XM1
      RHO=RH1
      XLAMB=XLAL
      RHOB=RHL
      THETA0=THET12
      WRITE(5,10)
10    FORMAT'3X,'SOLID 1-LIQUID INTERFACE')
      WRITE(5,11) THETA0
11    FORMAT(3X,'THETA0=',E12.5)
      CALL SOLLI(THETA0,XLAM,XMU,XLAMB,RHO,RHOB)
C     LAYER 4--SOLID 2-LIQUID INTERFACE
      XLAM=XLA2
      XMU=XM2
      RHO=RH2
      XLAMB=XLAL
      RHOB=RHL
      THETA0=THET32
      WRITE(5,12)
12    FORMAT(3X,'SOLID 2-LIQUID INTERFACE')
      WRITE(5,13) THETA0
13    FORMAT(3X,'THETA0=',E12.5)
      CALL SOLLI(THETA0,XLAM,XMU,XLAMB,RHO,RHOB)
      CL=CL2
      CALL CRCSUB(CL,THETA0,CL,YA)
      THET41=YA
      WRITE(5,14) THET41
14    FORMAT(3X,'THETA41=',E12.5)
C     LAYER 5---SOLID 2-SOLID 1 INTERFACE
      XLAM=XLA2
      XMU=XM2
      RHO=RH2
      XLAMB=XLA1
      XMUB=XM1
      RHOB=RH1
      THETA0=THET41
      WRITE(5,15)
15    FORMAT(3X,'SOLID 2-SOLID 1 INTERFACE')
      WRITE(5,16) THETA0
16    FORMAT(3X,'THETA0=',E12.5)
      CALL SOLID(THETA0,XMU,XLAM,XMUB,XLAMB,RHO,RHOB)
      CL=CL2
      CLB=CL1
      CALL CRCSUB(CL,THETA0,CLB,YC)
      THET35=YC
```

```
      WRITE(5,17) THET35
17    FORMAT(3X,'THETA35=',E12.5)
C     LAYER 6---SOLID 1-LIQUID INTERFACE
      XLAM=XLA1
      XMU=XM1
      RHO=RH1
      XLAMB=XLAL
      RHOB=RHL
      THETA0=THET35
      WRITE(5,18)
18    FORMAT(3X,'SOLID 1-LIQUID INTERFACE')
      WRITE(5,19) THETA0
19    FORMAT(3X,'THETA0= ',E12.5)
      CALL SOLLI(THETA0,XLAM,XMU,XLAMB,RHO,RHOB)
      STOP
      END
```

```
      SUBROUTINE WASO(THETA0,XLAM,XMUB,XLAMB,RHO,RHOB)
      CL=SQRT(XLAM*2.683/RHO)
      CLB=SQRT(((XLAMB+2.*XMUB))*2.683/RHOB)
      CTB=SQRT(XMUB*2.683/RHOB)
      CALL CRCSUB(CL,THETA0,CL,YA)
      THETA1=YA
      WRITE(5,2) THETA1
      CALL CRCSUB(CL,THETA0,CLB,YB)
      THETA3=YB
      WRITE(5,3) THETA3
      CALL CRCSUB(CL,THETA0,CTB,YC)
      THETA4=YC
      WRITE(5,4) THETA4
2     FORMAT(' THETA1=',F10.4)
3     FORMAT(' THETA3=',F10.4)
4     FORMAT(' THETA4=',F10.4)
      C11=-SIN(THETA1)
      C12=SIN(THETA3)
      C13=-COS(THETA4)
      C21=COS(THETA1)
      C22=COS(THETA3)
      C23=SIN(THETA4)
      C31=-XLAM/XLAM
      C32=CL*(XLAMB+2.*XMUB*COS(THETA3)*COS(THETA3))/(CLB*XLAM)
      C33=(CL*XMUB*SIN(2.*THETA4))/(XLAM*CTB)
      B1=SIN(THETA0)
      B2=COS(THETA0)
      B3=XLAM/XLAM
      WRITE(5,1) C11,C12,C13,B1
      WRITE(5,1) C21,C22,C23,B2
      WRITE(5,1) C31,C32,C33,B3
1     FORMAT(1X,E12.5,1X,E12.5,1X,E12.5,1X,E12.5)
      CALL D3(DETERM,C11,C12,C13,C21,C22,C23,C31,C32,C33)
      WRITE(5,10) DETERM
10    FORMAT(5X,'DETERM=',E12.5)
      CALL D3(DI,B1,C12,C13,B2,C22,C23,B3,C32,C33)
      X1=DI/DETERM
      WRITE(5,20) X1
20    FORMAT(5X,'A1/A0=',E12.5)
      CALL D3(DII,C11,B1,C13,C21,B2,C23,C31,B3,C33)
      X2=DII/DETERM
      WRITE(5,30) X2
30    FORMAT(5X,'A2/A0=',E12.5)
      CALL D3(DIII,C11,C12,B1,C21,C22,B2,C31,C32,B3)
      X3=DIII/DETERM
      WRITE(5,40) X3
40    FORMAT(5X,'A3/A0=',E12.5)
      RETURN
      END
```

```
      SUBROUTINE SOLLI(THETA0,XLAM,XMU,XLAMB,RHO,RHOB)
      CT=SQRT(XMU*2.683/RHO)
      CL=SQRT(((XLAM+2.*XMU)*2.683)/RHO)
      CLB=SQRT(XLAMB*2.683/RHO)
      CALL CRCSUB(CL,THETA0,CL,YA)
      THETA1=YA
      WRITE(5,2) THETA1
      CALL CRCSUB(CL,THETA0,CT,YB)
      THETA2=YB
      WRITE(5,3) THETA2
      CALL CRCSUB(CL,THETA0,CLB,YC)
      THETA3=YC
      WRITE(5,4) THETA3
2     FORMAT(' THETA1=',F10.4)
3     FORMAT(' THETA2=',F10.4)
4     FORMAT(' THETA3=',F10.4)
      C11=-SIN(THETA1)
      C12=SIN(THETA2)
      C13=SIN(THETA3)
      C21=COS(THETA1)
      C22=-SIN(THETA2)
      C23=COS(THETA3)
      B33=XLAM+2.*XMU*COS(THETA0)*COS(THETA0)
      C31=(XLAM+2.*XMU*COS(THETA1)*COS(THETA1))/B33
      C32=CL*XMU*SIN(2.*THETA2)/(CT*B33)
      C33=CL*XLAMB/(CLB*B33)
      B1=SIN(THETA0)
      B2=COS(THETA0)
      B3=(XLAM+2.*XMU*COS(THETA0)*COS(THETA0))/B33
      WRITE(5,1) C11,C12,C13,B1
      WRITE(5,1) C21,C22,C23,B2
      WRITE(5,1) C31,C32,C33,B3
      WRITE(5,5) B33
1     FORMAT(1X,E12.5,1X,E12.5,1X,E12.5,1X,E12.5)
5     FORMAT(' B33=',E12.5)
      CALL D3(DETERM,C11,C12,C13,C21,C22,C23,C31,C32,C33)
      WRITE(5,10) DETERM
10    FORMAT(5X,'DETERM=',E12.5)
      CALL D3(DI,B1,C12,C13,B2,C22,C23,B3,C32,C33)
      X1=DI/DETERM
      WRITE(5,20) X1
20    FORMAT(5X,'A1/A0=',E12.5)
      CALL D3(DII,C11,B1,C13,C21,B2,C23,C31,B3,C33)
      X2=DII/DETERM
      WRITE(5,30) X2
30    FORMAT(5X,'A2/A0=',E12.5)
      CALL D3(DIII,C11,C12,B1,C21,C22,B2,C31,C32,B3)
      X3=DIII/DETERM
      WRITE(5,40) X3
40    FORMAT(5X,'A3/A0=',E12.5)
      RETURN
      END
```

```
      SUBROUTINE SOLID(THETA0,XMU,XLAM,XMUB,XLAMB,RHO,RHOB)
      CL=SQRT((XLAM+2.*XMU)/RHO)
      CT=SQRT(XMU/RHO)
      CLB=SQRT((XLAMB+2.*XMUB)/RHOB)
      CTB=SQRT(XMUB/RHOB)
      CALL CRCSUB(CL,THETA0,CL,YA)
      THETA1=YA
      WRITE(5,1) THETA1
      CALL CRCSUB(CL,THETA0,CT,YB)
      THETA2=YB
      WRITE(5,2) THETA2
      CALL CRCSUB(CL,THETA0,CLB,YC)
      THETA3=YC
      WRITE(5,3) THETA3
      CALL CRCSUB(CL,THETA0,CTB,YD)
      THETA4=YD
      WRITE(5,4) THETA4
1     FORMAT(' THETA1=',E12.5)
2     FORMAT(' THETA2=',E12.5)
3     FORMAT(' THETA3=',E12.5)
4     FORMAT(' THETA4=',E12.5)
      C11=-SIN(THETA1)
      C12=-COS(THETA2)
      C13=SIN(THETA3)
      C14=-COS(THETA4)
      C21=COS(THETA1)
      C22=-SIN(THETA2)
      C23=COS(THETA3)
      C24=SIN(THETA4)
      B33=XMU
      C31=XMU*SIN(2.*THETA1)/B33
      C32=(XMU*CL*COS(2.*THETA2))/(CT*B33)
      C33=XMUB*CL*SIN(2.*THETA3)/(CLB*B33)
      C34=-XMUB*CL*COS(2.*THETA4)/(CTB*B33)
      B44=XLAM+2.*XMU*COS(THETA0)*COS(THETA0)
      C41=-(XLAM+2.*XMU*COS(THETA1)*COS(THETA1))/B44
      C42=XMU*CL*SIN(2.*THETA2)/(CT*B44)
      C43=CL*(XLAMB+2.*XMUB*COS(THETA3)*COS(THETA3))/(CLB*B44)
      C44=XMUB*CL*SIN(2.*THETA4)/(CTB*B44)
      B1=SIN(THETA0)
      B2=COS(THETA0)
      B3=XMU*SIN(2.*THETA0)/B33
      B4=(XLAM+2.*XMU*COS(THETA0)*COS(THETA0))/B44
      WRITE(5,5) C11,C12,C13,C14,B1
      WRITE(5,5) C21,C22,C23,C24,B2
      WRITE(5,5) C31,C32,C33,C34,B3
      WRITE(5,5) C41,C42,C43,C44,B4
5     FORMAT(1X,E12.5,1X,E12.5,1X,E12.5,1X,E12.5,1X,E12.5)
      CALL D4(DETERM,C11,C12,C13,C14,C21,C22,C23,C24,C31,
     XC32,C33,C34,C41,C42,C43,C44)
      WRITE(5,10) DETERM
10    FORMAT(5X,'DETERM=',E12.5)
```

```
      CALL D4(DI,B1,C12,C13,C14,B2,C22,C23,C24,
     XB3,C32,C33,C34,B4,C42,C43,C44)
      X1=DI/DETERM
      WRITE(5,20) X1
20    FORMAT(5X,'A1/A0=',E12.5)
      CALL D4(DII,C11,B1,C13,C14,C21,B2,C23,C24,C31,
     XB3,C33,C34,C41,B4,C43,C44)
      X2=DII/DETERM
      WRITE(5,30) X2
30    FORMAT(5X,'A2/A0=',E12.5)
      CALL D4(DIII,C11,C12,B1,C14,C21,C22,B2,C24,
     XC31,C32,B3,C34,C41,C42,B4,C44)
      X3=DIII/DETERM
      WRITE(5,40) X3
40    FORMAT(5X,'A3/A0=',E12.5)
      CALL D4(DIV,C11,C12,C13,B1,C21,C22,C23,B2,C31,
     XC32,C33,B3,C41,C42,C43,B4)
      X4=DIV/DETERM
      WRITE(5,50) X4
50    FORMAT(5X,'A4/A0=',E12.5)
      RETURN
      END
```

```
      SUBROUTINE D4(D,A11,A12,A13,A14,A21,A22,A23,A24,A31,A32,
     XA33,A34,A41,A42,A43,A44)
      CALL D3(DA,A22,A23,A24,A32,A33,A34,A42,A43,A44)
      CALL D3(DB,A21,A23,A24,A31,A33,A34,A41,A43,A44)
      CALL D3(DC,A21,A22,A24,A31,A32,A34,A41,A42,A44)
      CALL D3(DD,A21,A22,A23,A31,A32,A33,A41,A42,A43)
      D=A11*DA-A12*DB+A13*DC-A14*DD
      RETURN
      END
C
      SUBROUTINE D3(D,A11,A12,A13,A21,A22,A23,A31,
     XA32,A33)
      CALL D2(DE,A22,A23,A32,A33)
      CALL D2(DF,A21,A23,A31,A33)
      CALL D2(DG,A21,A22,A31,A32)
      D=A11*DE-A12*DF+A13*DG
      RETURN
      END
C
      SUBROUTINE D2(D,A11,A12,A21,A22)
      D=A11*A22-A12*A21
      RETURN
      END
*


      SUBROUTINE CRCSUB(A,B,C,Y)
      X=A*SIN(B)/C
      Y=X+(X**3.)/6.+3.*(X**5.)/40.+5.*(X**7.)/112.
     X+35.*(X**9.)/576.
      RETURN
      END
```

APPENDIX B

TWO-DIMENSIONAL CORRELATION OF TWO LINES X = Y = UNIFORM TRANSLATION

```
      DIMENSION A(100,10--), AX(10),AY(10),DI(1,100)
      READ(7,10) N,M,NP
      READ(7,11) DELX
10    FORMAT(3I4)
11    FORMAT(F10.4)
      DO 12 I=1,N,1
      DO 13 J=1,N,1
13    A(I,J)=0.0
12    CONTINUE
      READ(7,20) (DI(1,I),I=1,100)
20    FORMAT(F10.4)
      DO 3 I=1,100,1
      A(I,1)=DI(1,I)
      A(1,I)=DI(1,I)
3     CONTINUE
      DO 5 I=1,99,1
      DO 6 J=1,99,1
6     A(I+1,J+1)=A(I+1,1)*A(1,J+1)/3.
5     CONTINUE
      K=N-M
      DO 9 MM=0,K,M
      NN=MM
      DO 7 I=1,M,1
      AX(I)=A(MM+1,I+NN)
      AY(I)=A(I+MM,NN+1)
7     CONTINUE
      CALL CORRI(A,AX,AY,N,M,NP)
9     CONTINUE
      STOP
      END
```

```
C
      SUBROUTINE CORRI(A,AX,AY,N,M,IC)
      WRITE(5,30)
30    FORMAT(5X,'CORRI')
      DIMENSION A(100,100),AX(10),AY(10)
      S2=10E20
      C2=10E20
      INM=0
      IMN=0
      ICNM=N-M
      DO 2 J=1,ICNM,1
      DO 1 L=0,ICNM,1
      S=0.0
      C=0.0
      DO 3 II=1,M,1
      S1=AX(II)-A(J,II+L)
      C1=AY(II)-A(II+L,J)
      S=S+S1*S1
      C=C+C1*C1
3     CONTINUE
      IF(S.LT.S2) INM=L
      IF(S.LT.S2) S2=S
      IF(C.LT.C2) IMN=L
      IF(C.LT.C2) C2=C
1     CONTINUE
2     CONTINUE
      DX=0.001*FLOAT(INM*IC)
      DY=0.001*FLOAT(IMN*IC)
      WRITE(5,9) S2
9     FORMAT(5X,'CORRELATION-X=',E12.5)
      WRITE(5,7) C2
7     FORMAT(5X,'CORREALTION-Y=',E12.5)
      WRITE(5,8) DX,DY
8     FORMAT(5X,'DX=',F10.3,3X,'DY=',F10.3)
      RETURN
      END
```

```
CORRI
CORRELATION-X= 0.00000E+00
CORREALTION-Y= 0.00000E+00
DX=      0.000    DY=      0.000
CORRI
CORRELATION-X= 0.00000E+00
CORREALTION-Y= 0.00000E+00
DX=      0.005    DY=      0.005
CORRI
CORRELATION-X= 0.00000E+00
CORREALTION-Y= 0.00000E+00
DX=      0.010    DY=      0.010
CORRI
CORRELATION-X= 0.00000E+00
CORREALTION-Y= 0.00000E+00
DX=      0.015    DY=      0.015
CORRI
CORRELATION-X= 0.00000E+00
CORREALTION-Y= 0.00000E+00
DX=      0.020    DY=      0.020
CORRI
CORRELATION-X= 0.00000E+00
CORREALTION-Y= 0.00000E+00
DX=      0.025    DY=      0.025
CORRI
CORRELATION-X= 0.00000E+00
CORREALTION-Y= 0.00000E+00
DX=      0.030    DY=      0.030
CORRI
CORRELATION-X= 0.00000E+00
CORREALTION-Y= 0.00000E+00
DX=      0.035    DY=      0.035
CORRI
CORRELATION-X= 0.00000E+00
CORREALTION-Y= 0.00000E+00
DX=      0.040    DY=      0.040
CORRI
CORRELATION-X= 0.00000E+00
CORREALTION-Y= 0.00000E+00
DX=      0.045    DY=      0.045
CORRI
CORRELATION-X= 0.00000E+00
CORREALTION-Y= 0.00000E+00
DX=      0.050    DY=      0.050
```

```
CORRI
CORRELATION-X= 0.00000E+00
CORREALTION-Y= 0.00000E+00
DX=      0.055    DY=      0.055
CORRI
CORRELATION-X= 0.00000E+00
CORREALTION-Y= 0.00000E+00
DX=      0.060    DY=      0.060
CORRI
CORRELATION-X= 0.00000E+00
CORREALTION-Y= 0.00000E+00
DX=      0.065    DY=      0.065
CORRI
CORRELATION-X= 0.00000E+00
CORREALTION-Y= 0.00000E+00
DX=      0.070    DY=      0.070
CORRI
CORRELATION-X= 0.00000E+00
CORREALTION-Y= 0.00000E+00
DX=      0.075    DY=      0.075
CORRI
CORRELATION-X= 0.00000E+00
CORREALTION-Y= 0.00000E+00
DX=      0.080    DY=      0.080
CORRI
CORRELATION-X= 0.00000E+00
CORREALTION-Y= 0.00000E+00
DX=      0.085    DY=      0.085
CORRI
CORRELATION-X= 0.00000E+00
CORREALTION-Y= 0.00000E+00
DX=      0.090    DY=      0.090
CORRI
CORRELATION-X= 0.00000E+00
CORREALTION-Y= 0.00000E+00
DX=      0.095    DY=      0.095
 --
```

REFERENCES

1. Ranson, W. F., "Use Holographic Interferometry to Determine the Surface Displacement Components of a Deformed Body," University of Illinois, Urbana, Illinois, TAM Report No. 348, August 1971.

2. Ranson, W. F., D. C. Holloway and C. E. Taylor, "A Neoteric Interferometer for Use in Holographic Photoelasticity," Experimental Mechanics, Vol. II, No. 10, October 1972.

3. Ranson, W. F., W. H. Peters and W. F. Swinson, "Non-Linear Plate Deformation Measurements Using Speckle Reference Beam Holography," Proceedings of 14th Annual Meeting of the Society of Engineering Science, November 1977.

4. Kinariwala, V. R., W. F. Ranson, and W. F. Swinson, "Stress Analysis of Vibrating Compressor Blades," Technical Report ME-UC-7405, Dept. of Mechanical Engineering, Auburn University, Auburn, Alabama, February 1976.

5 Ranson, W. F. and W. F. Swinson, "Speckle Patterns for Measuring Displacements Described as Diffraction Gratings," Proceedings of 12th Annual Meeting of the Society of Engineering Science, University of Texas at Austin, October 1975.

6. Mullinix, B. R., W. F. Ranson, and W. F. Swinson, "The Impact Pressure Distribution of a Hypervelocity Ramdrop," US Army Missile Command Technical Report RL-TR-72, December 1972.

7. Schaeffel, J. A., W. F. Ranson, B. R. Mullinix, and W. F. Swinson, "Computer Aided Optical Nondestructive Flaw Detection System for Composite Materials," US Army Missile Research and Development Command Technical Report T-78-5, September 1977.

8. Goodman, J. W., "Statistical Properties of Laser Speckle Patterns," in Laser Speckle and Related Phenomena, edited by J. C. Dainty (Springer-Verlag, Heidelberg, 1975), Vol. 9 (Topics in Applied Physics), pp. 9-75.

9. Goodman, J. W., "Some Fundamental Properties of Speckle," Jour. Optical Soc. Amer., Vol. 66, No. 11, pp. 1145-1150, Nov. 1976.

10. Strutt, J. W. (Lord Rayleigh), "On the Resultant of A Large Number of Vibrations of the Same Pitch and of Arbitrary Phase," Philos. Mag. 10, 73-78, (1880).

11. Schaeffel, John A., "Acoustical Speckle Interferometry," Mechanical Engineering Department, Auburn University, Auburn, Alabama, (1978).

12. Schaeffel, J. A., W. F. Ranson, and W. F. Swinson, "Acoustical Speckle Interferometry," Experimental Mechanics, Vol. 20, No. 4, 109-117, April 1980.

13. Achenbach, J. D., Wave Propagation in Elastic Solids, American Elsevier Pub. Co., New York, (1973).

14. Kräutkramer, J., Arch. Eisenhuettenw - 30, 693-703, (1959).

15, Gericke, O. R., "Determination of the Geometry of Hidden Defeces by Ultrasonic Pulse Analysis Testing," J. Acoust. Soc. Am., 35, 364-368, (1963).

16. Gericke, O. R., "Ultrasonic Spectroscopy," Chapter 2 in Research Techniques in Non-destructive Testing, R. S. Sharpe, Ed., Academic Press, London, (1970).

17. Brown, A. F., Ultrasonics II, 202-210, (1973).

18. Lloyd, E. A., British Non-Ferrous Metals Research Assoc. paper S 150/30/13, (1972).

19. Sachse, W. "Ultrasonic Spectroscopy of a Fluid-Filled Cavity in an Elastic Solic," J. Acoust, Soc. Am., Vol. 56, No. 3, September 1974.

20. Strutt, J. W. (Lord Rayleigh), "Theory of Sound," (Dover, New Jersey, 1945), Vol. II, p. 272.

21. Pao, Y. H. and Mow, C. C., "Diffraction of Elastic Waves and Dynamic Stress Concentrations," Crane, Russak, New York, (1973).

22. White, R. M., "Elastic Wave Scattering at a Cylindrical Discontinuity in a Solid," J. Acoust. Soc. Am., 30, 771-785, (1958).

23. *Goodman*, R. R., R. E. Bunney, and S. W. Marshall, "Observation of Circumferential Waves of Solid Aluminum Cylinders," J. Acoust. Soc. Am., 42, 523-524, (1967)

24. Neubauer, W. G., "Experimental Measurement of 'Creeping' Waves on Solid Aluminum Cylinders in Water Using Pulses, J. Acoust. Soc. Am., 44, 298-299, (1968).

25. Neubauer, W. G., "Experimental Observation of Three Types of Pulsed Circumferential Waves on Solid Aluminum Cylinders," J. Acoust. Soc. Am., 44, 1150-1152, (1958).

26. Neubauer, W. G., "Pulsed Circumferential Waves on Aluminum Cylinders in Water," J. Acoust. Soc. Am., 45, 1134-1144, (1969).

27. Bunney, R. E., R. R. Goodman, and S. W. Marshall, "Rayleigh and Lamb Waves on Cylinders," J. Acoust. Soc. Am., 46, 1223-1233, (1969).

28. Shachse, W. and C. T. Chian, "Determination of the Size and Mechanical Properties of a Cylindrical Fluid Inclusion in an Elastic Solid," Materials Evaluation, 33, 81-88, (1975).

29. Bifulco, F. and W. Sachse, "Ultrasonic Pulse Spectroscopy of a Solid Inclusion in an Elastic Solid," Ultrasonics, 10, 113-116, (1975).

30. Rhodes, Deborah J., and Wolfgang Sachse, "Arrival Times of Scattered Ultrasonic Signals from a Solid Inclusion in an Elastic Material," J. Acoustic. Soc. Am., 65 (5), May 1979.

31. Blinka, J., and W. Sachse, "Application of Ultrasonic-pulse-spectroscopy Measurements to Experimental Stress Analysis," Experimental Mechanics, 448-453, December 1976.

32. Ensminger, D., "Ultrasonics - The Low and High - Intensity Applications," Marrel Dekker, Inc., (1973).

33. Hilderbrand, B. P. B. B. Branden, "An Introduction to Acoustical Holography," Plenum Press, (1972).

34. Toknoka, T. and Y. Iwashimizu, "Acoustical Birefringence of Ultrasonic Waves in Deformed Isotropic Elastic Materials," Int. J. Solids Structure, 4, 338-389, (1968).

35. Toupin, R. A., and B. Bernstein, "Sound Waves in Deformed Perfectly Elastic Materials-Acoustoelastic Effect," J. Acoust. Soc. Am., 33, 216-225, (1960).

36. Nelson, N. Hsu, "Acoustical Birefringence and the Use of Ultrasonic Wave for Experimental Stress Analysis," Experimental Mechanics, 169-176, May 1974.

37. Granato, A., J. Deklerk, and R. Truell, phys. Rev., 108, 895, (1957).

38. Hikata, A., B. Chick, Elbaum, and R. Truell, Appl. Phys. Letters 205, (1963).

39. Truell, R., and H. Hikata, "Ultrasonic Methods in the Study of Plastic Deformation," Physical Acoustics, III A, 199-221, Ed W. P. Mason, (Academic Press., New York), (1966).

40. Thomson, W., "Transmission of Elastic Waves Through A Stratified Medium," J. Appl. Phys., 21, 89-93, (1950).

41. Brekhovskikh, L. M., "Wave in Layered Media," (Academic Press, New York), (1960).

42. Shaw, R. P., and P. Bugl, "Transmission of Plane Waves through Layered Linear Viscoelastic Media," J. Acoust. Soc. Am., 46, 649-654, (1969).

43. Folds, D. L., and C. D. Loggins, "Transmission and Reflection of Ultrasonic Waves in Layered Media," J. Acoust. Soc. Am., 62, 1102-1109, (1977).

44. Lahart, M. J., "Optical Correlation with Magnification and Rotation," J. Opt. Soc. Amer., pp. 319-325, March 1970.

45. Mostafavi, H., and F. W. Smith, "Image Correlation with Geometric Distortion - Part I: Acquisition Performance," IEEE Trans. Aerosp. Electron. Syst., Vol. AES-14, pp. 487-493, May 1978.

46. _____, "Image Correlation with Geometric Distorion - Part II: Effect on Local Accuracy," IEEE Trans. Aerosp. Electron. Syst., Vol. AES-14, pp. 494-501, May 1978.

47. _____, "Optimal Window Functions for Image Correlation in the Presence of Geometric Distortion," IEEE Trans. Aco., Sp., and Sig. Proc., Vol. ASSP-27, pp. 163-169, April 1979.

48. Novozhilov, V. V., Theory of Elasticity, Office of Technical Services. US Department of Commerce, Washington, DC.

DISTRIBUTION

	No. of Copies
Director USA Mobility Equipment Research and Development Center Coating and Chemical Laboratory ATTN: STSFB-CL Aberdeen Proving Ground, Maryland 21005	1
Commander Edgewood Arsenal ATTN: SAREA-TS-A Aberdeen Proving Ground, Maryland 21010	1
Commander Picatinny Arsenal ATTN: SARPA-TS-S, Mr. M. Costello Dover, New Jersey 07801	1
Commander Rock Island Arsenal Research and Development ATTN: 9320 Rock Island, Illinois 61201	1
Commander Watervliet Arsenal Watervliet, New York 12189	1
Commander US Army Aviation Systems Command ATTN: DRSAV-EE -MT, Mr. Vollmer St. Louis, Missouri 63166	1 1
Commander US Army Aeronautical Depot Maintenance Center (Mail Stop) Corpus Christi, Texas 78403	1
Commander US Army Test and Evaluation Command ATTN: DRSTE-RA Averdeen Proving Ground, Maryland 21005	1
Commander ATTN: STEAP-MT Aberdeen Proving Ground, Maryland 21005	1
Technical Library Naval Ordnance Station Indian Head, Maryland 20640	1

DISTRIBUTION (Continued)

	No. of Copies
Chief Bureau of Naval Weapons Department of the Navy Washington, DC 20390	1
Chief Bureau of Ships Department of Navy Washington, DC 20315	1
Naval Research Laboratory ATTN: Dr. M M. Krafft Code 8430 Washington, DC 20375	1
Commander Wright Air Development Division ATTN: ASRC Wright-Patterson AFB, Ohio 45433	1
Director Air Force Materiel Laboratory ATTN: AFML-DO-Library Wright-Patterson AFB, Ohio 45433	1
Director Army Materials and Mechanics Research Center ATTN: DRXMR-PL -MT, Mr. Farrow Watertown, Massachusetts 02172	1 1
Commander White Sands Missile Range ATTN: STEWS-AD-L White Sands Missile Range, New Mexico 88002	1
Jet Propulsion Laboratory California Institute of Technology ATTN: Library/Acquisitions 111-113 4800 Oak Grove Drive Pasadena, California 91103	1
Sandia Laboratories ATTN: Library P. O. Box 969 Livermore, California 94550	1

DISTRIBUTION (Continued)

	No. of Copies
Commander US Army Air Defense School ATTN: ATSA-CD-MM Fort Bliss, Texas 79916	1
Commander US Army Materiel Development and Readiness Command ATTN: DRCMT Washington, DC 20315	1
Headquarters SAC/NRI (Stinfo Library) Offutt Air Force Base, Nebraska 68113	1
Commander Rock Island Arsenal ATTN: SARRI-KLPL-Technical Library Rock Island, Illinois 61201	1
Commander (Code 233) Naval Weapons Center ATTN: Library Division China Lake, California 93555	1
Department of the Army US Army Research Office ATTN: Information Processing Office P. O. Box 12211 Research Triangle Park, North Carolina 27709	1
Commander US Army Research Office ATTN: DRXRO-PW, Dr. R. Lontz P. O. Box 12211 Research Triangle Park, North Carolina 27709	2
US Army Research and Standardization Group (Europe) ATTN: DRXSN-E-RX, Dr. Aldred K. Nodoluha Box 65 FPO New York 09510	2
Headquarters Department of the Army Office of the DCS for Research Development and Acquisition Room 3A474, The Pentagon ATTN: DAMA-ARZ Washington, DC 20310	2

DISTRIBUTION (Concluded)

	No. of Copies
US Army Materiel Systems Analysis Activity ATTN: DRXSY-MP Aberdeen Proving Ground, Maryland 21005	1
IIT Research Institute ATTN: GACIAC 10 West 35th Street Chicago, Illinois 60616	1
ADTC (DLDSL) Eglin Air Force Base, Florida 32542	1
University of California Los Alamos Scientific Laboratory ATTN: Reports Library P. O. Box 1663 Los Alamos, New Mexico 87545	1
Commander US Army Materiel Development and Readiness Command ATTN: DRCRD DRCDL 5001 Eisenhower Avenue Alexandria, Virginia 22333	1 1
Director Defense Advanced Research Projects Agency 1400 Wilson Bouldvard Arlington, Virginia 22209	1
DRSMI-LP, Mr. Voight	1
DRSMI-R, Dr. Kobler	1
-RL, Mr. Comus	1
-RLA, Mr. Pettey	1
-RLA, Mr. Schaeffel	50
-RPR	3
-RPT (Reference Copy)	1
(Record Set)	1

END

DATE
FILMED

5 -83

DTIC